

Direct dark matter searches - Test of the Big Bounce Cosmology

Yeuk-Kwan E. Cheung¹ J.D. Vergados^{1,2,3}

¹Department of Physics, Nanjing University, 22 Hankou Road, Nanjing, China 210093

²TEI of Western Macedonia, Kozani, Gr 501 00, Greece and KAIST, 291 Daehak-ro, Yuseong-gu, Daejeon 305-701, Republic of Korea

³University of Ioannina, Ioannina, Gr 451 10, Greece

E-mail: cheung@nju.edu.cn, vergados@uoi.gr

Abstract. We consider the possibility of using dark matter particle's mass and its interaction cross section as a smoking gun signal of the existence of a Big Bounce at the early stage in the evolution of our currently observed universe. A study of dark matter production in the pre-bounce contraction and the post bounce expansion epochs of this universe reveals a new venue for achieving the observed relic abundance of our present universe. Specifically, it predicts a characteristic relation governing a dark matter mass and interaction cross section and a factor of $1/2$ in thermally averaged cross section, as compared to the non-thermal production in standard cosmology, is needed for creating enough dark matter particle to satisfy the currently observed relic abundance because dark matter is being created during the pre-bounce contraction, in addition to the post-bounce expansion. As the production rate is lower than the Hubble expansion rate information of the bounce universe evolution is preserved. Therefore once the value of dark matter mass and interaction cross section are obtained by direct detection in laboratories, this alternative route becomes a signature prediction of the bounce universe scenario. This leads us to consider a scalar dark matter candidate, which if it is light, has important implications on dark matter searches.

Keywords: Dark matter, WIMP, direct detection, Bounce Universe, WIMP-nucleus scattering, event rates, modulation, Debris Flows

ArXiv ePrint: [1410.5710](https://arxiv.org/abs/1410.5710)

To the memory of Tan Lu (1932.2.23 – 2014.12.3).

Contents

1	Introduction	1
2	The big bounce universe scenario	4
3	The particle model.	5
4	The formalism for the WIMP-nucleus differential event rate	8
5	Some results on differential rates	11
6	Some results on total rates	12
7	Discussion and conclusions	15
	References	28

1 Introduction

The combined MAXIMA-1 [1],[2],[3], BOOMERANG [4],[5] DASI [6] and COBE/DMR Cosmic Microwave Background (CMB) observations [7] imply that the Universe is flat [8] and that most of the matter in the Universe is Dark [9], i.e. exotic. These results have been confirmed and improved by the recent WMAP [10] and Planck [11] data. Combining the data of these quite precise measurements one finds:

$$\Omega_b = 0.0456 \pm 0.0015, \quad \Omega_{\text{CDM}} = 0.228 \pm 0.013, \quad \Omega_\Lambda = 0.726 \pm 0.015$$

(the more recent Planck data yield a slightly different combination $\Omega_{\text{CDM}} = 0.274 \pm 0.020$, $\Omega_\Lambda = 0.686 \pm 0.020$). It is worth mentioning that both the WMAP and the Planck observations yield essentially the same value of $\Omega_m h^2$, but they differ in the value of h , namely $h = 0.704 \pm 0.013$ (WMAP) and $h = 0.673 \pm 0.012$ (Planck). Since any “invisible” non exotic component cannot possibly exceed 40% of the above Ω_{CDM} [12], exotic (non baryonic) matter is required and there is room for cold dark matter candidates or WIMPs (Weakly Interacting Massive Particles).

Even though there exists firm indirect evidence for a halo of dark matter in galaxies from the observed rotational curves, see e.g. the review [13], it is essential to directly detect such matter in order to unravel the nature of the constituents of dark matter.

The possibility of such detection, however, depends on the nature of the dark matter constituents and their interactions.

Since the WIMP’s are expected to be extremely non-relativistic, with average kinetic energy $\langle T \rangle \approx 50 \text{ keV} (m_{\text{WIMP}}/100 \text{ GeV})$, they are not likely to excite the nucleus. So they

can be directly detected mainly via the recoiling of a nucleus (A, Z) in elastic scattering. The event rate for such a process can be computed from the following ingredients [14]: i) The elementary nucleon cross section. ii) knowledge of the relevant nuclear matrix elements obtained with as reliable as possible many body nuclear wave functions, iii) knowledge of the WIMP density in our vicinity and its velocity distribution.

In the standard nuclear recoil experiments, first proposed more than 30 years ago [15], one has to face the problem that the reaction of interest does not have a characteristic feature to distinguish it from the background. So for the expected low counting rates the background is a formidable problem. Some special features of the WIMP-nuclear interaction can be exploited to reduce the background problems. Such are:

i) the modulation effect: this yields a periodic signal due to the motion of the earth around the sun. Unfortunately this effect, also proposed a long time ago [16] and subsequently studied by many authors [14, 17–25], is small and becomes even smaller than 2% due to cancelations arising from nuclear physics effects,

ii) backward-forward asymmetry expected in directional experiments, i.e. experiments in which the direction of the recoiling nucleus is also observed. Such an asymmetry has also been predicted a long time ago [26], but it has not been exploited, since such experiments have been considered very difficult to perform. Some progress has, however, has recently been made in this direction and they now appear feasible [26–38]. In such experiments the event rate depends on the direction of observation. In the most favorable direction, opposite to the sun’s direction of motion, is comparable to the standard event rate. The sensitivity of these experiments for various halo models has also been discussed [31, 32]. Furthermore we should mention that in such experiments [27, 30, 38] all events are counted. If some interesting events can be found, they can be established by further analyzing them by the direction of the observed recoils.

An essential ingredient in direct WIMP detection is the WIMP density in our vicinity and, especially, the WIMP velocity distribution. The dark matter in the solar neighborhood is commonly assumed to be smoothly distributed in space and to have a Maxwellian velocity distribution. Some of the calculations have considered various forms of phenomenological non symmetric velocity distributions [39–42] [23, 30, 31] and some of them even more exotic dark matter flows like the late infall of dark matter into the galaxy, i.e caustic rings [43–47] and Sagittarius dark matter [48].

In addition to the above models very recently it was found that the velocity distributions measured in high resolution numerical simulations exhibit deviations from the standard Maxwell-Boltzmann assumption, especially at large velocities [49, 50]. Furthermore a distinction was between a velocity structure that is spatially localized, such as streams [51, 52], and that which is spatially homogenized, which was designated as “debris flow” [53]. Both streams and debris flows arise from the disruption of satellites that fall into the Milky Way, but differ in the relative amount of phase-mixing that they have undergone. Implications of streams [54] and the debris flows in direct dark matter searches have also been considered [55], [56].

In the present paper we will address the following points:

- The implications scalar WIMPs on the expected event rates. The interest in such a WIMP has recently been revived due to a new scenario of dark matter production

in bounce cosmology [57, 58] in which the authors point out the possibility of using dark matter as a probe of a big bounce at the early stage of cosmic evolution. A model independent study of dark matter production in the contraction and expansion phases of the Big Bounce reveals a new venue for achieving the observed relic abundance in which dark matter was produced completely out of chemical equilibrium¹. A characteristic relation, Fig. 2, comes out of the model independent analysis. This is to be contrasted

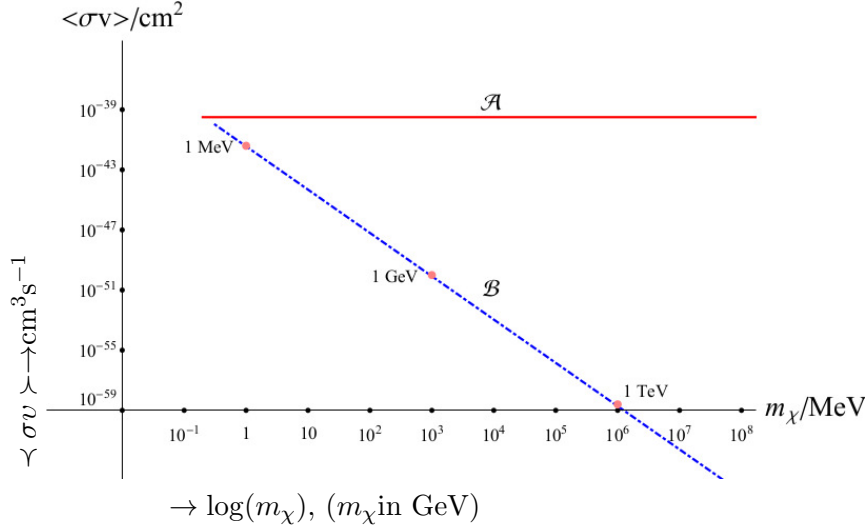


Figure 1: The cross section $\langle \sigma v \rangle$ as a function of the WIMP mass. In the standard cosmology it is a constant (solid line), but it varies considerably in the bounce universe scenario (dotted line)

with the straight line (cross-section being independent of dark matter mass) of the standard cosmology.

Once DM mass and its coupling constant with ordinary matter are extracted from experimental data we can check if they obey the predicted relation. In this way, this alternative route of dark matter production in bounce cosmology can be used to test the bounce cosmos hypothesis.

- In order to settle the issues raised above we will compute the differential and total event rates in a variety of targets such as those employed in XENON [60, 61], CoGENT [62], DAMA [63, 64], LUX [65], CDMSII [66], CRESST [67] and PICASSO [68, 69]. For this study we will consider not only the standard Maxwell Boltzmann distribution but also the effects of debris flows [55] on these rates including the modulation due to annual motion of the Earth [70].

¹ Note that in Standard Cosmology, non-thermal production of dark matter could also happen, which has been utilized in [59] to test non-standard cosmologies proposed in that era. The relation among dark matter mass and cross section predicted in the standard cosmology is, however, generically different from the predictions from the bounce universe scenario. One of the major differences is that—for non-thermal production—in standard cosmology the relic abundance of dark matter depends substantially—at the leading order—on reheating temperature, T_{RH} , as was first pointed in [59]. Whereas in the bounce universe scenario, the relic abundance does not depend on the bounce temperature, T_b , at the leading order; instead it appears at the sub-leading orders of the relic abundance [57].

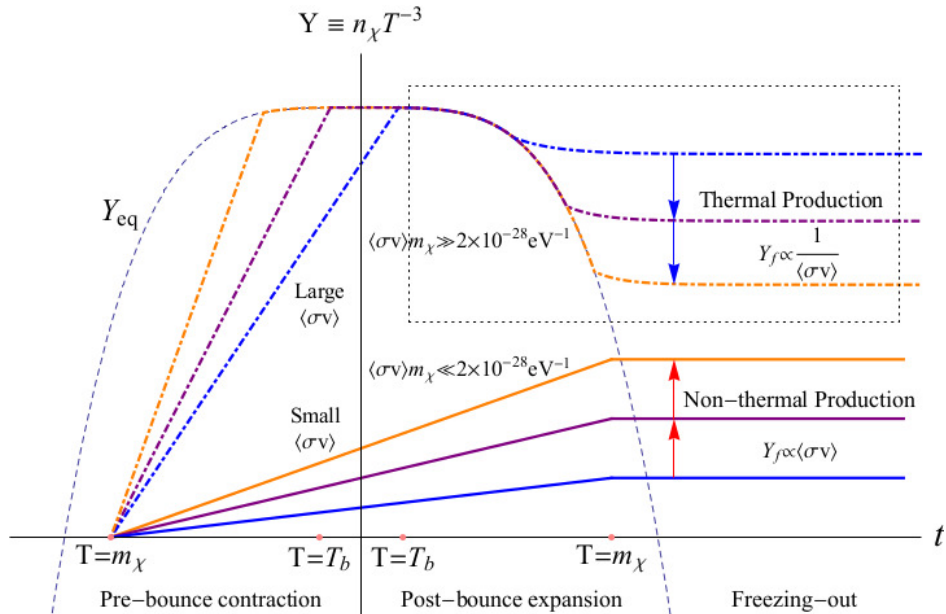


Figure 2: A schematic plot of the time evolution of dark matter in a generic bounce universe scenario. Two pathways of producing dark matter yet satisfying current observations thermal production (which is indistinguishable from standard cosmology) and non-thermal production (characteristic to bounce universe) are illustrated. The horizontal axis indicates both the time, t , as well as the temperature, T , of the cosmological background.

In any case, regardless of the validity of the big bounce universe scenario, the scalar WIMPs have the characteristic feature that the elementary cross section in their scattering off ordinary quarks is increasing as the WIMPs get lighter, which leads to an interesting experimental feature, namely it is expected to enhance the event rates at low WIMP mass. In the present calculation we will adopt this view and study its implications in direct dark matter searches compared to other types of WIMPs, such as the neutralinos, which we will call standard.

Scalar WIMP's can occur in particle models. Examples are i) In Kaluza-Klein theories for models involving universal extra dimensions (for applications to direct dark matter detection see, e.g., [71]). In such models the scalar WIMPs are characterized by ordinary couplings, but they are expected to be quite massive. ii) very light particles [72] not relevant to the ongoing WIMP searches ii) Scalar WIMPS such as those considered previously in various extensions of the standard model [73], which can be quite light and long lived protected by a discrete symmetry. Thus they are viable cold dark matter candidates.

2 The big bounce universe scenario

Recently a stable as well as scale-invariant power spectrum of primordial density perturbations is finally obtained [74, 75] in the bounce universe scenario. The “Bounce Cosmology” postulates that there exists a phase of matter-dominated contraction before the Big Bang [76] during which the matter content of the universe comes into thermal contact—resulting in a

scale invariant spectrum—before a subsequent expansion after the big bounce. In view of this development we are motivated to work out further experimental or observational predictions the Bounce Universe model [57, 58] (See also [77].)². Our study is model independent of a particular bounce model and our predictions are of particle physics nature and can be tested independently at LHC or dark matter direct detections, outside of the cosmological context.

A signature prediction from the bounce universe: By investigating the production process of dark matter in the pre-bounce contraction and the post-bounce expansion epochs of a generic bounce universe, we find that, in the big bounce scenario, dark matter production can be extended beyond the Big Bang, as shown in Fig. 1 (compare the dotted and solid lines). Furthermore an out-of-thermal-equilibrium production of dark matter is allowed, which encodes information of early universe evolution, marked the non-thermal production” in Fig. 2. Specifically it predicts a relation governing a dark matter mass and interaction cross section, depicted by the solid line in Fig. 1. This behavior reflects a mass dependence of the cross-section, characteristic of a scalar type WIMP. As shown in Fig. 2, we divide the bounce (See [92, 93] for recent reviews.) schematically into three stages to facilitate a model independent analysis [57, 58].

3 The particle model.

If the WIMP is a scalar [94–97] particle χ interacting with another scalar ϕ via a quartic coupling the cross section $\prec \sigma v \succ$ for the process:

$$\phi + \phi \rightarrow \chi + \chi \quad (3.1)$$

in the center of mass system is given by:

$$\prec \sigma v \succ = \frac{1}{16\pi} \frac{\lambda^2}{m_\chi^2} \frac{\sqrt{s - 4m_\chi^2} \sqrt{s}}{4m_\phi^2}, \quad \sqrt{s} \geq 2m_\chi \quad (3.2)$$

In the limit in which $m_\phi \gg m_\chi$ and $\sqrt{s} \approx 2m_\phi$ we find:

$$\prec \sigma v \succ \approx \frac{1}{16\pi} \frac{\lambda^2}{m_\chi^2} \quad (3.3)$$

We will assume in this work that ϕ is the Higgs scalar discovered at LHC.

If the WIMP is a scalar particle χ interacting with another scalar ϕ via a quartic coupling the cross section $\prec \sigma v \succ$ for the process:

$$\phi + \phi \rightarrow \chi + \chi \quad (3.4)$$

in the center of mass system is given by:

$$\prec \sigma v \succ = \frac{1}{16\pi} \frac{\lambda^2}{m_\chi^2} \frac{\sqrt{s - 4m_\chi^2} \sqrt{s}}{4m_\phi^2}, \quad \sqrt{s} \geq 2m_\chi \quad (3.5)$$

²Use of observational data from WMAP, Planck and BICEP2 has been made to test bounce models [78–91].

In the limit in which $m_\phi \gg m_\chi$ and $\sqrt{s} \approx 2m_\phi$ we find:

$$\prec \sigma v \succ \approx \frac{1}{16\pi} \frac{\lambda^2}{m_\chi^2} \quad (3.6)$$

which is in essential agreement with the expression after Eq. (4) given previously [57, 58], but with different assumptions. For the scalar WIMP- quark scattering the relevant Feynman diagram is shown in Fig. 3.

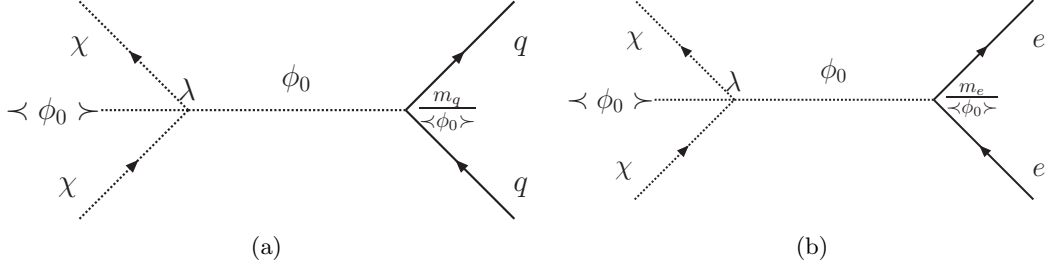


Figure 3: The quark - scalar WIMP scattering mediated by a scalar particle. Note that the amplitude is independent of the vacuum expectation value $\prec \phi_0 \succ$ of the scalar (a). The corresponding diagram for electron scalar- WIMP scattering (b)

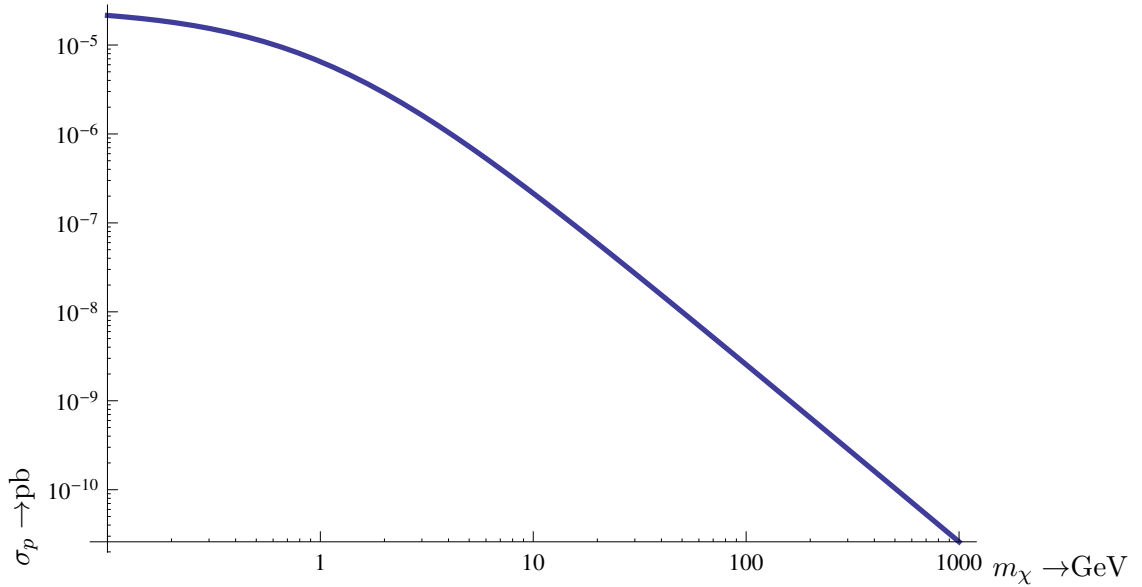


Figure 4: The nucleon cross section as a function of the WIMP mass in the case the WIMP is a scalar particle. The overall scale was adjusted to fit the cross section of 10^{-8} pb obtained from the exclusion plots of XENON100 at 50 GeV.

The resulting nucleon cross section is given by:

$$\sigma_p = \frac{1}{4\pi} \frac{\lambda^2 m_p^2 (\mu_r^2)}{m_\phi^4} \frac{1}{m_\chi^2} \left(\sum_q f_q \right)^2 = \frac{1}{4\pi} \frac{\lambda^2 m_p^2}{m_\phi^4} \frac{1}{(1 + m_\chi/m_p)^2} \left(\sum_q f_q \right)^2 \quad (3.7)$$

Note that the vacuum expectation value $\prec \phi_0 \succ$ in the quartic coupling is canceled by the Yukawa coupling of the Higgs with the quarks. The parameter f_q is related to the probability of finding the quark q in the nucleon:

$$f_q = \frac{\prec m_q q \bar{q} \succ}{m_N} \quad (3.8)$$

i.e. the heavy quarks become important, even though the probability of finding them in the nucleon is small. If the scalar is the Higgs particle discovered at LHC, $\lambda = 1/2$, $m_\phi = 126$ GeV, one finds:

$$\sigma_p = \sigma_0 \left(1 + \frac{m_\chi}{m_p} \right)^{-2}, \quad \sigma_0 = 6 \times 10^{-11} m_p^{-2} \left(\sum_q f_q \right)^2 \quad (3.9)$$

The value of $\sum_q f_q$, of course, can vary, but a reasonable, albeit rather optimistic, value of 0.5 is acceptable [98, 99], [100]. Thus

$$\sigma_0 \approx 0.009 \text{ pb} \rightarrow \sigma_p \approx 3 \times 10^{-6} \text{ pb} \left(\frac{50}{m_\chi (\text{GeV})} \right)^2, \quad \text{for } m_\chi \gg m_p \quad (3.10)$$

This for $m_\chi = 50 \text{ GeV}$ this value is quite a bit bigger than the limit extracted from the current experimental searches. So in our treatment we have fixed the parameter σ_0 in the nucleon cross section so that for a WIMP mass of 50 GeV we get the limit extracted from experiments, e.g. 10^{-8} pb from XENON100 [61, 101]. The thus obtained cross section is exhibited in Fig. 4. It is interesting to compare the behavior of this cross section with that of the relic abundance of the BUS shown in Fig. 1. We note that this mass dependence of the cross section of scalar WIMPs, i.e. exhibiting an enhancement in the low WIMP mass regime, may favor the searches at low energy transfers.

In the case of light WIMPs, another interesting domain of the BUS (Fig. 1), one finds that WIMPs with energy less than 100 MeV cannot produce a detectable recoiling nucleus, but they could produce electrons [102] with energies in the tens of eV, which could be detected with current mixed phase detectors [103]. We are not, however, going to discuss further this possibility in this work. If the WIMP is a scalar particle, however, it can interact in a similar pattern with other fermions, e.g. electrons. The relevant Feynman diagram is shown in Fig. 3.

For WIMPs with mass in the range of the electron mass, both the WIMP and the electron are not relativistic. So the expression for elementary electron cross section is similar to that of hadrons, i.e. it is now given by:

$$\sigma_e = \frac{1}{4\pi} \frac{\lambda^2 m_e^2}{m_\phi^4} \left(\frac{m_e m_\chi}{m_e + m_\chi} \right)^2 \frac{1}{m_\chi^2} \approx 8.0 \times 10^{-7} \text{ pb} \left(\frac{1}{1 + m_\chi/m_e} \right)^2, \quad (3.11)$$

obtained using the same values of λ and ϕ as above. This is a respectable size cross section dependent on the ratio m_χ/m_e . In this case one must consider electron recoils, but the highest possible electron energy is about 1.5 eV and the WIMP mass must be greater than 0.3 electron masses. So the detection of WIMPs with mass around the electron mass requires another type of detector and it will not be discussed further in the present work.

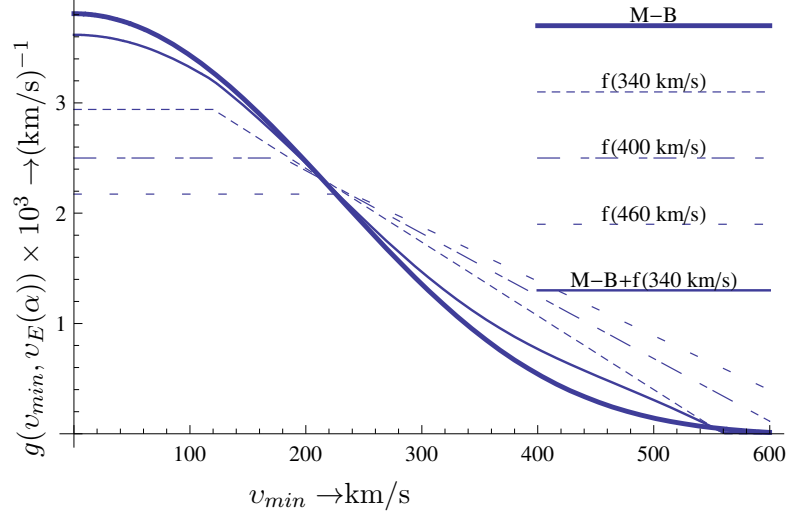


Figure 5: The function $g(v_{min})$ as a function of v_{min} in the local frame considered in this work in the case of the traditional M-B distribution as well as the indicated velocity flows[55].

4 The formalism for the WIMP-nucleus differential event rate

The most interesting quantity which depends on the velocity distribution is the quantity $g(v_{min})$. For the M-B distribution in the local frame it is defined as follows:

$$g(v_{min}, v_E(\alpha)) = \frac{1}{(\sqrt{\pi}v_0)^3} \int_{v_{min}}^{v_{max}} e^{-(v^2 + 2v \cdot v_E(\alpha) + v_E^2(\alpha))/v_0^2} v dv d\Omega \quad (4.1)$$

For isotropic debris flows [55] it is given by:

$$g(v_{min}, v_E(\alpha)) = \int_{v_{min}} \frac{f(v)}{v} dv, \quad f(v) = \begin{cases} \frac{v}{2v_{flow}v_E(\alpha)}, & v_{flow} - v_E(\alpha) < v < v_{flow} + v_E(\alpha) \\ 0, & \text{otherwise} \end{cases} \quad (4.2)$$

These functions are shown in Fig. 5.

In what follows we will find it useful to expand $g(v_{min}, v_E(\alpha))$ in powers of δ , the ratio of the Earth's velocity around the sun divided by the velocity v_0 of the sun around the galaxy (220km/s). Keeping terms up to linear in $\delta \approx 0.135$ and expressing everything in dimensionless variables we obtain:

$$v_0 g(v_{min}, v_E(\alpha)) = \Psi_0(x) + \Psi_1(x) \cos \alpha, \quad x = \frac{v_{min}}{v_0} \quad (4.3)$$

where $\Psi_0(x)$ represents the quantity relevant for the average rate, $\Psi_1(x)$, which is proportional to δ , represents the modulation and α is the phase of the Earth ($\alpha = 0$ around June 3rd). In the case of the flows they were derived from the semi-analytic approximations of simulations as discussed by Spergel and co-workers [55].

In the case of a M-B distribution these functions have been given previously [104]. For

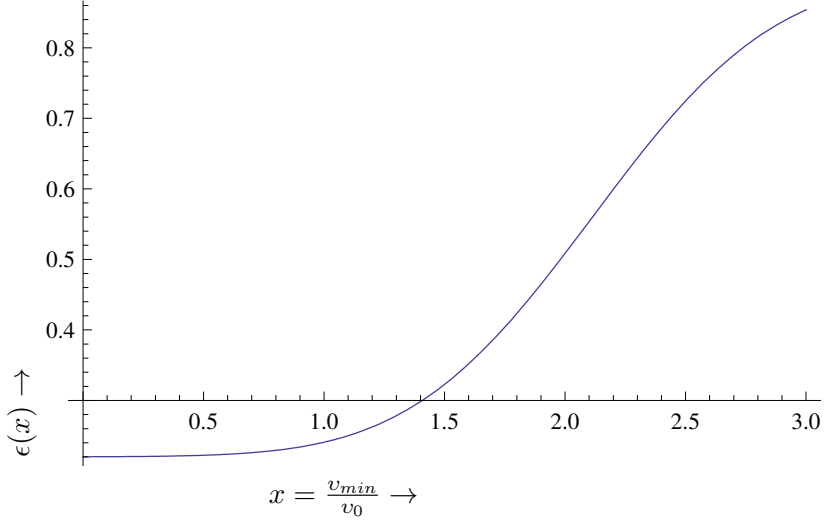


Figure 6: The function $\epsilon(x)$, $x = v_{min}/v_0$ as a function of x , which gives a possible combination of a M-B distribution and debris flows[55].

isotropic debris flows one finds:

$$\Psi_0(x) = \begin{cases} \frac{1}{y_f} & 0 < x < y_f - 1 \\ \frac{1+y_f-x}{2y_f} & y_f - 1 < x < 1 + y_f \\ 0 & x > 1 + y_f \end{cases}, \quad y_f = \frac{v_{flow}}{v_0} \quad (4.4)$$

$$\Psi_1(x) = \delta \begin{cases} 0 & 0 < x < y_f - 1 \\ \frac{x-y_f}{4y_f} & y_f - 1 < x < 1 + y_f \\ 0 & x > 1 + y_f \end{cases}, \quad y_f = \frac{v_{flow}}{v_0} \quad (4.5)$$

We note that the variable x depends on the nuclear recoil energy E_R as well as the WIMP-nucleus reduced mass. As we shall see below there is an additional dependence of the rates on E_R coming from the nuclear form factor.

At Earth-frame velocities greater than 450 km/s, debris flow comprises more than half of the dark matter at the Sun's location, and up to 80% at even higher velocities[55]. In the VL2 simulation, the combination of debris flows and standard M-B is very well fit by the function

$$\epsilon(x) = 0.22 + 0.34 \left(\text{erf} \left(x \frac{220}{185} - \frac{465}{185} \right) + 1 \right) \quad (4.6)$$

This function is exhibited in Fig. 6. In this case we find:

$$\Psi_i(x) \rightarrow (1 - \epsilon(x)) \Psi_i^{MB}(x) + \epsilon(x) \Psi_i^f(x), \quad i = 0, 1 \quad (4.7)$$

The functions $\Psi_0(x)$ and $\Psi_1(x)$ are exhibited in Fig. 7. As expected in the case of the flows $\Psi_0(x)$ falls off linearly for large values of x . Note that in all cases $\Psi_1(x)$ takes both positive and negative values, which affects the location of the maximum of the modulated rate as a function of α , depending on the target and the WIMP mass. We will explore this effect of the different distributions in direct experiments searching any time dependence of the rates.

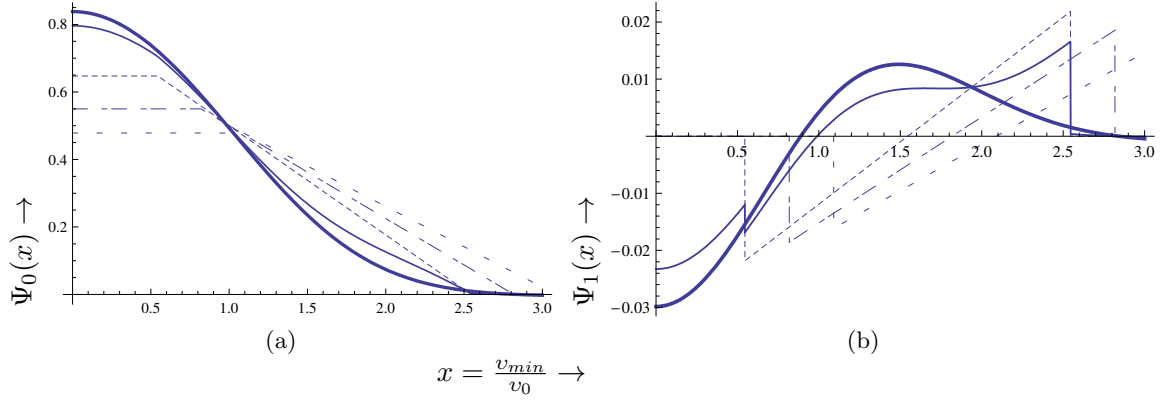


Figure 7: The functions $\Psi_0(x)$ and $\Psi_1(x)$ as a function of $x = v_{min}/v_0$. Note that these functions have been computed at $\alpha = 0$, i.e. the average local velocity. Note also that the variable x depends on the nuclear recoil energy E_R as well as the WIMP-nucleus reduced mass. Otherwise the labeling of the curves is the same as that of Fig. 5.

Once these functions are known the formalism to obtain the direct detection rates is fairly well known (see e.g. the recent reviews [105, 106]). So we will briefly discuss its essential elements here. The differential event rate can be cast in the form:

$$\frac{dR}{dE_R}|_A = \frac{dR_0}{dE_R}|_A + \frac{d\tilde{H}}{dE_R}|_A \cos \alpha \quad (4.8)$$

where the first term represents the time averaged (non modulated) differential event rate, while the second gives the time dependent (modulated) one due to the motion of the Earth (see below). Furthermore

$$\begin{aligned} \frac{dR_0}{dE_R}|_A &= \frac{\rho_\chi}{m_\chi} \frac{m_t}{Am_p} \sigma_n \left(\frac{\mu_r}{\mu_p} \right)^2 \sqrt{\langle v^2 \rangle} A^2 \frac{1}{Q_0(A)} \frac{dt}{du}, \\ \frac{d\tilde{H}}{dE_R}|_A &= \frac{\rho_\chi}{m_\chi} \frac{m_t}{Am_p} \sigma_n \left(\frac{\mu_r}{\mu_p} \right)^2 \sqrt{\langle v^2 \rangle} A^2 \frac{1}{Q_0(A)} \frac{dh}{du} \end{aligned} \quad (4.9)$$

with μ_r (μ_p) the WIMP-nucleus (nucleon) reduced mass, A is the nuclear mass number and σ_n is the elementary WIMP-nucleon cross section. m_χ is the WIMP mass and m_t the mass of the target. Furthermore one can show that

$$\frac{dt}{du} = \sqrt{\frac{2}{3}} a^2 F^2(u) \Psi_0(a\sqrt{u}), \quad \frac{dh}{du} = \sqrt{\frac{2}{3}} a^2 F^2(u) \Psi_1(a\sqrt{u}) \quad (4.10)$$

with $a = (\sqrt{2}\mu_r b v_0)^{-1}$, v_0 the velocity of the sun around the center of the galaxy and b the nuclear harmonic oscillator size parameter characterizing the nuclear wave function. u is the energy transfer Q in dimensionless units given by

$$u = \frac{E_R}{Q_0(A)}, \quad Q_0(A) = [m_p A b^2]^{-1} = 40 A^{-4/3} \text{ MeV} \quad (4.11)$$

and $F(u)$ is the nuclear form factor. In the present calculation they were obtained in context of the nuclear shell model in the spirit of [107] (for the spin induced process see, e.g. [107, 108]).

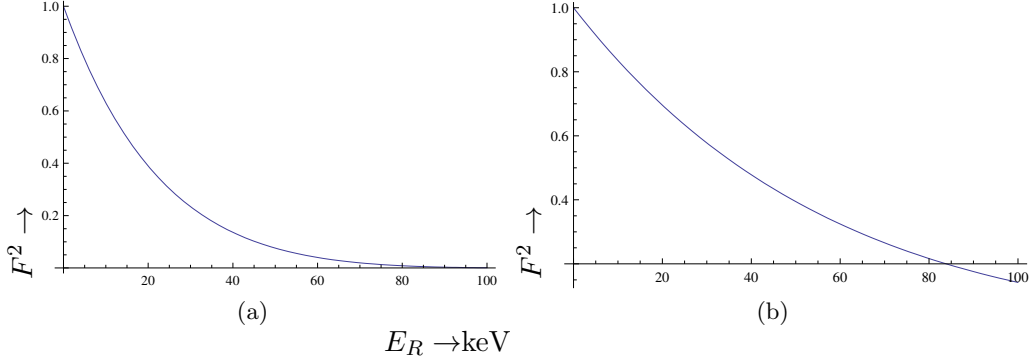


Figure 8: The square of the nuclear form factor for a heavy target, e.g. ^{127}I (a) and an intermediate target, e.g. ^{73}Ge (b). For light targets the effect of the form factor is small.

The form factor is important in the case of a heavy target and large WIMP mass, i.e. for large recoil energies (see Fig. 8).

Note that the parameter a depends both on the WIMP, the target and the velocity distribution. Note also that for a given energy transfer E_R the quantity u depends on A . Sometimes one writes the differential rate as:

$$\frac{dR}{dE_R}|_A = \frac{\rho_\chi}{m_\chi} \frac{m_t}{Am_p} \sigma_n \left(\frac{\mu_r}{\mu_p} \right)^2 \sqrt{\langle v^2 \rangle} A^2 \frac{1}{Q_0(A)} \left(\frac{dt}{du} (1 + H(a\sqrt{E_R/Q_0(A)}) \cos \alpha) \right) \quad (4.12)$$

In this formulation $H(a\sqrt{E_R/Q_0(A)})$, the ratio of the modulated to the non modulated differential rate, gives the relative differential modulation amplitude. It coincides with the ratio $\Psi_1(a\sqrt{E_R/Q_0(A)})/\Psi_0(a\sqrt{E_R/Q_0(A)})$, i.e. it is independent of the nuclear form factor and depends only on the reduced mass and the velocity distribution. It is thus the same for both the coherent and the spin mode. Note that it can take both positive and negative values, which affects the location of the maximum of the modulated rate as a function of α . For the convenience of the analysis of experiments, however, we will present our results in the form of Eq. 4.9.

5 Some results on differential rates

We will apply the above formalism in the case of I and Na, which are components of the target NAI used in the DAMA experiment [63, 64] and Ge employed, e.g. by the CoGeNT experiment [62]. The results for the Xe target [60] are similar to those for I and for the ^{19}F target [68, 69] are similar to those for Na. The differential rates $\frac{dR}{dQ}|_A$ and $\frac{d\tilde{H}}{dQ}|_A$, for each component ($A = 127$ and $A = 23$) and for $A = 73$ are exhibited in Fig. 9-20. The nuclear form factor has been included (for a heavy target, like ^{127}I or ^{131}Xe , its effect is sizable even for an energy transfer [70] of 10 keV, see Fig. 8).

By comparing the plots of the differential event rates of scalar WIMPs to the standard ones we find that the shapes are the same, but for low mass the scalar WIMPs lead to much larger event rates. So we will restrict the discussion on the shape of these plots to the results obtained for standard WIMPs.

The introduction of debris flows makes a small contribution at low energy transfers. As expected[55] it tends to increase the differential rate at high energy transfers. This is particularly true for light small WIMP-nucleus reduced mass (see Figs 9, 13 and 17). One, however, does not see any particular signature in the shape of the resulting curve. Furthermore the event rate in this region is about five times smaller than the maximum. One, however, observes an interesting pattern concerning the time varying (modulated) part of the rate (see Figs 11, 15 and 19). For a heavy target, like ^{127}I or ^{131}Xe , it is not surprising that, for WIMPs with relatively large mass, the modulation becomes negative, i.e. the rate becomes minimum in June 3rd, for all models considered here. For low WIMP masses, however, the sign of the modulation due to the flows is opposite to that of the M-B distribution. Thus the use of the light target nucleus ^{19}F , combined with the low detection threshold of 1.7 keV for recoil nuclei, makes PICASSO particularly sensitive to low mass dark matter particles and gives it also some leverage in the low mass region of the spin independent sector. The present stage of the experiment[109] is approaching the sensitivity to challenge or confirm the claims of seasonal modulations by the DAMA[64] and CoGeNT[62] experiments. A similar situation arises in the case of an intermediate target, like ^{73}Ge . Here the M-B distribution yields a negative value only for very low energy transfers. The situation becomes most interesting in the case of a light target, see Fig. 15. Here, with the possible exception of quite low energy transfers, which perhaps are below or very near threshold, the M-B distribution yields a positive modulation amplitude, i.e. a maximum on June 3rd, while the result of debris flows is to cause a change in sign as one moves to high energy transfers. Also in this case the modulation amplitude tends to increase as the energy transfer increase, while the corresponding contribution due to the M-B distribution tends to decrease. We should remark though that the total rate (average+modulated) tends to decrease at high momentum transfers. We should also stress that we have presented here the absolute modulate rate (events per kg target per year). The relative modulated amplitude (the ratio of the time varying rate divided by the time averaged) maybe larger.

The above results, as we will see in the next section, have important implications in the total event rates.

Sometimes, as is the case for the DAMA experiment, the target has many components. In such cases the above formalism can be applied as follows:

$$\frac{dR}{dQ}|_A \rightarrow \sum_i X_i \frac{dR}{dQ}|_{A_i}, \quad u \rightarrow u_i, \quad X_i = \text{the fraction of the component } A_i \text{ in the target} \quad (5.1)$$

We will not, however, pursue such an analysis.

6 Some results on total rates

For completeness and comparison we will briefly present our results on the total rates. Integrating the differential rates discussed in the previous section we obtain the total rate R , adding the corresponding time averaged rate R_0 and the total modulated rate \tilde{H} , given by:

$$R = R_0 + \tilde{H} = \frac{\rho_\chi}{m_\chi} \frac{m_t}{Am_p} \left(\frac{\mu_r}{\mu_p} \right)^2 \sqrt{\langle v^2 \rangle} A^2 \sigma_n t (1 + h \cos \alpha), \quad (6.1)$$

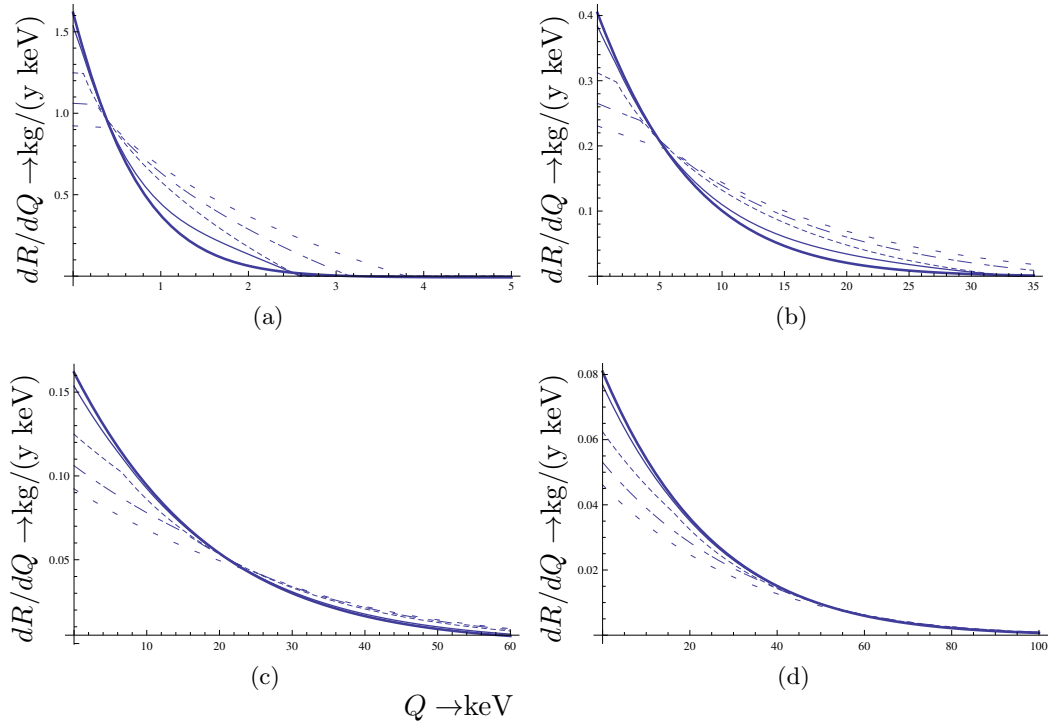


Figure 9: The differential rate $\frac{dR}{dQ}$, as a function of the recoil energy for a heavy target, e.g. ^{127}I assuming a nucleon cross section of 10^{-8}pb . Panels (a) (b), (c) and (d) correspond to 5, 20, 50 and 100 GeV WIMP masses. Otherwise the notation is the same as that of Fig. 5.

with

$$t = \int_{Q_{th}/Q_0(A)}^{(y_{\max}/a)^2} \frac{dt}{du} du, \quad h = \frac{1}{t} \int_{Q_{th}/Q_0(A)}^{(y_{\max}/a)^2} \frac{dh}{du} du. \quad (6.2)$$

y_{\max} is the maximum velocity allowed by the distribution and $Q_{th}(A)$ is the energy cut off imposed by the detector.

The obtained results for quantities R_0 and h are exhibited in Figs 21-23 assuming a nucleon cross section of 10^{-8}pb (at $m_\chi=50$ GeV for a scalar WIMP). For a standard WIMP in the case of a heavy target the average event rate attains the maximum value of 30 events per kg of target per year at a WIMP mass of 25 GeV, while for heavy WIMPS it eventually falls to about 5 kg/y at 500 GeV (to a good approximation it falls inversely proportional to the WIMP mass above the 200 GeV). For an intermediate target we get 15 kg/y at 25 GeV, with an asymptotic value of 4 kg/y. For a light target the maximum becomes 2.5 kg/y at 20 GeV. Again the asymptotic value at 500 GeV is about 1/5 of the maximum. The situation is very different for a scalar WIMP. At small WIMP masses the event rate becomes huge. The effect will appear less dramatic, if the value of 10^{-8}pb is fitted to a much smaller WIMP mass, since it will manifest itself for masses below that choice, but it is there. At high WIMP masses the event rate falls more rapidly with the mass. The relative modulation amplitude, however, being the ratio of the time dependent rate divided by the time averaged rate is the same for both types of WIMPs.

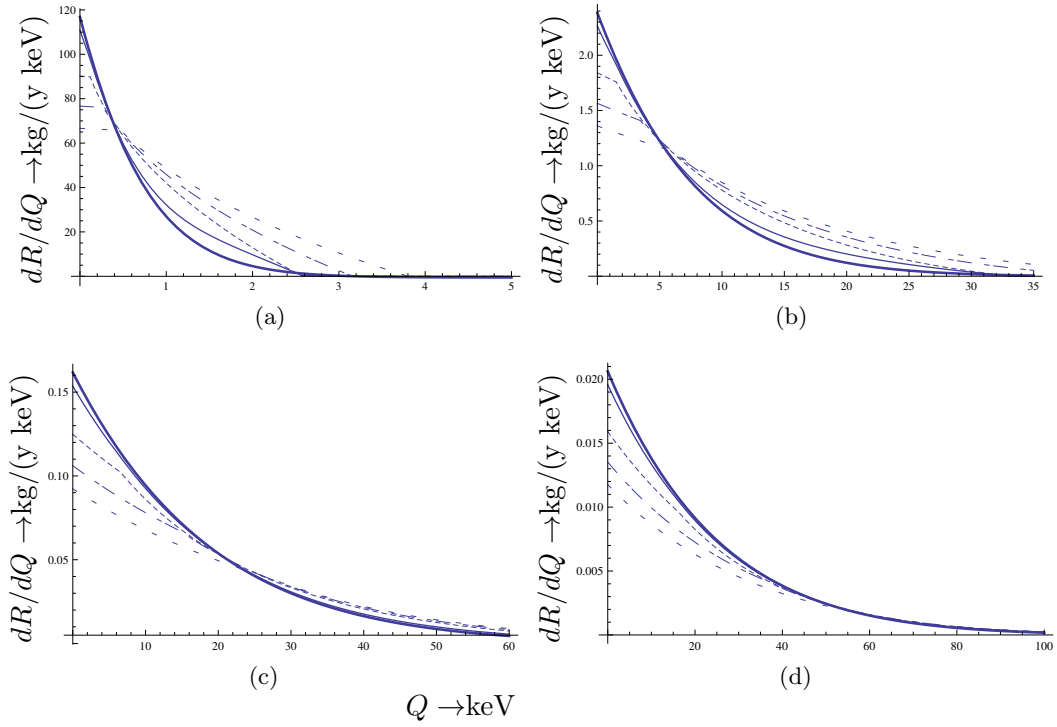


Figure 10: The same as in Fig. 9 for a scalar WIMP assuming a nucleon cross section $(50/m_\chi)^2 \times 10^{-8} \text{pb}$.

To understand this behavior we should mention that the WIMP mass dependence comes from three sources.

- From the momentum transfer, yielding a contribution to the event rate proportional to the square of μ_r (the WIMP-nucleus reduced mass), which vanishes quadratically for zero WIMP mass.
- From the WIMP particle density in our vicinity, which is inversely proportional to the mass (from the rotation curves we infer the density, not the number of particles per unit volume). In the limit of large WIMP mass this wins out over the previous one, since the reduced mass then is essentially the mass of the nucleus. For small WIMP mass the combination of these terms vanishes linearly.
- For scalar WIMPS we have the additional mass dependence coming from the elementary cross section $\sigma_n \propto (1 + m_\chi/m_p)^{-2}$ as we have seen.

We thus conclude that even in the case for a scalar WIMP at a low mass the total rate is proportional to

$$R \propto \mu_r^2 \frac{1}{m_\chi} \frac{1}{(1 + m_\chi/m_p)^2} \rightarrow 0 \text{ as } m_\chi \rightarrow 0.$$

It is clear that, as far as the time average rates R_0 are concerned, the debris flows do not exhibit any characteristic signature to differentiate them from the standard M-B distribution.

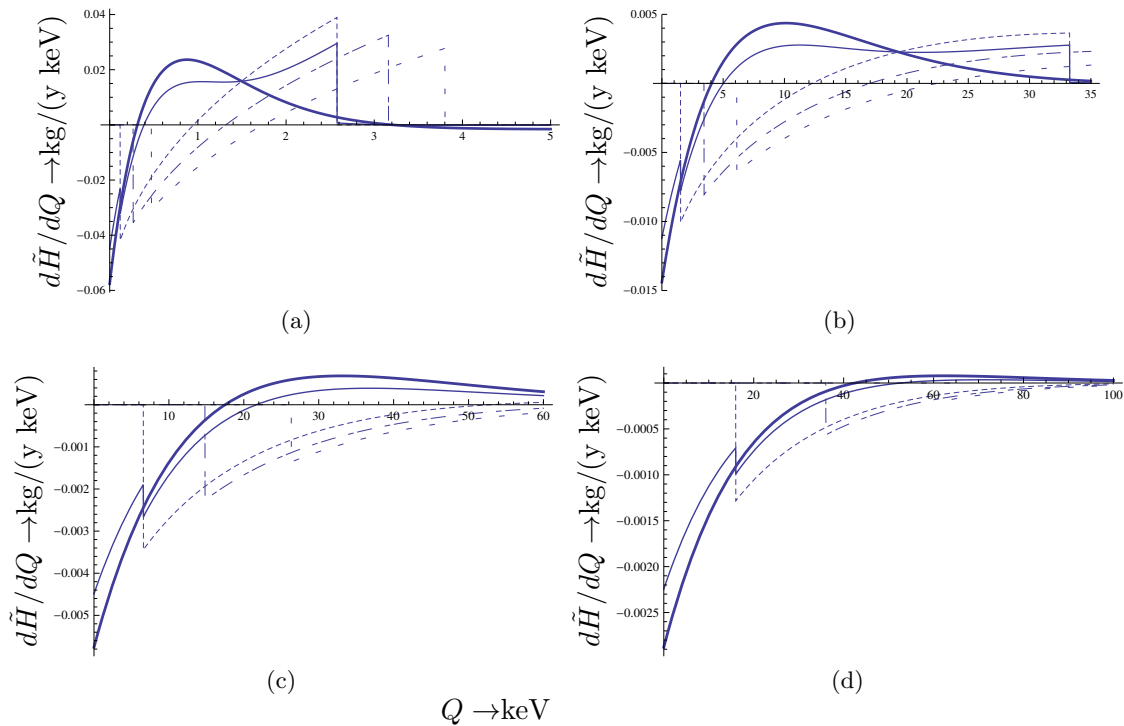


Figure 11: The differential rate $\frac{d\tilde{H}}{dQ}$, as a function of the recoil energy for a heavy target, e.g. ^{127}I assuming a nucleon cross section of 10^{-8}pb . Panels (a) (b), (c) and (d) correspond to 5, 20, 50 and 100 GeV WIMP masses. Otherwise the notation is the same as that of Fig. 5.

The relative modulation amplitude h , however, exhibits a very interesting feature, namely, if caused by the flows, it is negative for all targets, even for the light ones, and in the entire WIMP mass range (minimum in June). On the other hand if it is caused by the M-B distribution it is positive in the case of light targets regardless of the WIMP mass. It is also positive for intermediate/heavy targets, if the WIMPs are relatively light. Then the maximum occurs on June 3rd as expected. It becomes negative only for relatively heavy WIMPs. Thus it is an experimental challenge to measure the small time dependence of the event rate with a relative difference between the maximum and the minimum of $2h \approx 4\%$. From such data on both light and heavy targets, if and when they become available, one may be able: i) to get a hint about the size of the WIMP mass and ii) infer the existence of flows.

7 Discussion and conclusions

In the present paper we first obtained results on the differential event rates, both modulated and time averaged. We have considered a new type of viable WIMP, namely a scalar WIMP, motivated by the Big Bounce Scenario of Cosmology (BUS). We then compared the obtained results with the standard WIMP with a nucleon cross section independent of the WIMP

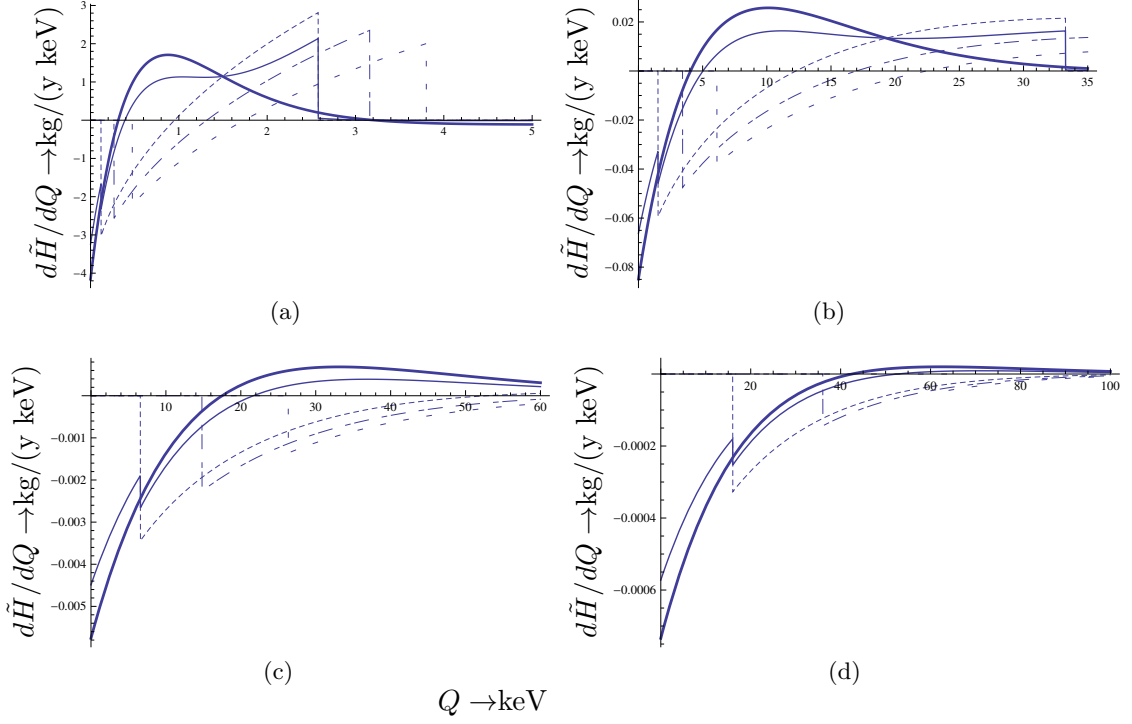


Figure 12: The same as in Fig. 11 for a scalar WIMP assuming a nucleon cross section $(50/m_\chi)^2 \times 10^{-8} \text{pb}$.

mass. We found that:

- The nucleon cross section is a decreasing function as the WIMP mass increases. This is in line with the predictions of BUS (compare Fig. 1 and Fig. 4).
- The above mass dependence leads to an increase of the rates at a low WIMP mass. This may be good news for the low threshold experiments using light nuclear targets (DM-TPC, NEWAGE, DRIFT, MIMAC etc), which are sensitive to low mass WIMPs.
- The maximum of the total event rate is shifted to a much lower regime, which may require a lower recoil energy threshold than currently achieved.
- As far as we know this behavior of the cross section is not excluded by the current data. In fact it may aid the analysis of the experimental data in the low WIMP mass regime even though there is a tendency for model independent analysis of the data, as e.g. in DAMA/LIBRA [110].
- It may be interesting to draw exclusion plots with this new nucleon cross section and extract the value of σ_0 entering Eq. (3.9).
- It may also help explaining the large cross section extracted from the recent CRESST data [67], if they persist.

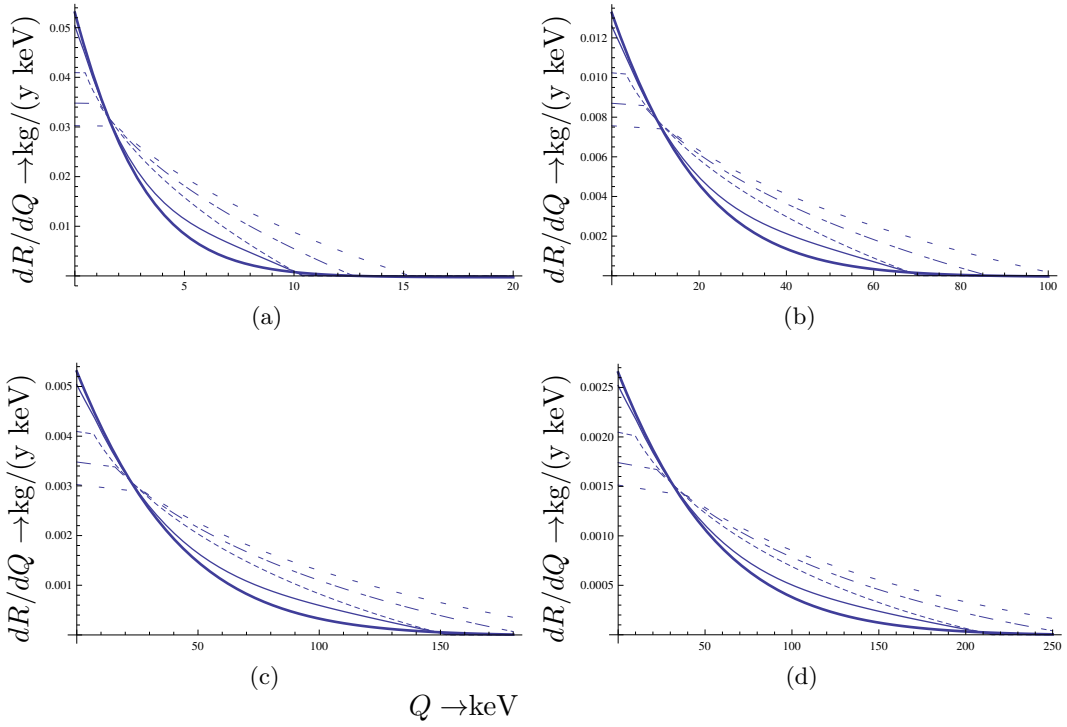


Figure 13: The differential rate $\frac{dR}{dQ}$, as a function of the recoil energy for a light target, e.g. ^{23}Na assuming a nucleon cross section of 10^{-8}pb . Panels (a) (b), (c) and (d) correspond to 5, 20, 50 and 100 GeV WIMP masses. Otherwise the notation is the same as that of Fig. 5.

We also examined the sensitivity of the obtained results to the velocity distribution (the nuclear form factor is the same of both types of WIMPs). We considered both a standard M-B velocity distribution and also models, which extend it, e.g. debris flows, which have also been considered [55], [56] previously. Thus we found out that:

- The flows indeed enhance the time averaged rates at relatively high energy transfers compared to the M-B distribution, at the expense of the corresponding rates at low energy transfers. All rates, however, fall as the energy transfer increases. This fall is only partially due to the velocity distribution. It is also caused by the nuclear form factor, in particular in the case of heavy targets. Anyway this behavior cannot be exploited to differentiate between them, since the WIMP mass is not known. Thus the time averaged rates do not provide a clear signature to differentiate the debris flows from the standard M-B distribution.
- The differential time dependent (modulated) rates provide such a signature, the sign of the modulation amplitude, which determines the position of the maximum. At sufficiently low energy transfer both the M-B and the debris flows favor a negative sign (minimum on June 3rd), with the flows insisting on such behavior more strongly and exhibiting it all the way to high energy transfers. So if the flows are there this signature may be seen even with detectors, which do not have a very low energy threshold.

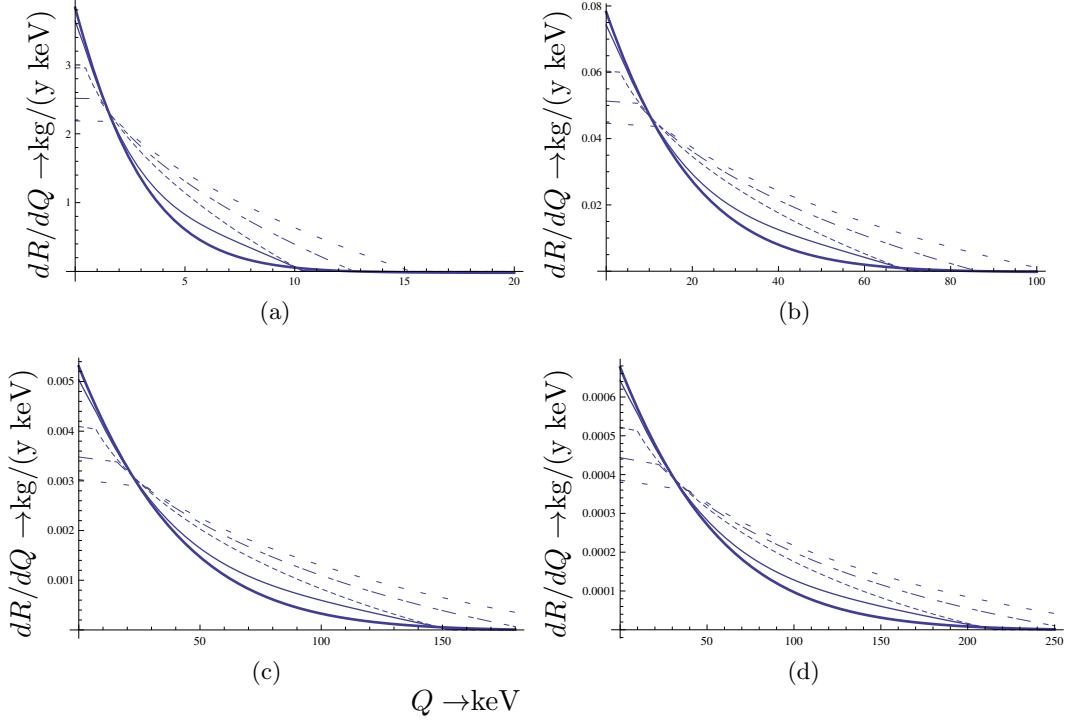


Figure 14: The same as in Fig. 10 in the case of a light target, e.g. ^{23}Na .

- For the M-B distribution this behavior is manifested for an energy which depends on the target and the WIMP mass (see Figs 11,12,15,16,19, 20). Thus e.g. for a heavy target this recoil energy is 0.5, 5, 20 and 40 keV. This recoil energy is the same for both types of WIMPs, only the rate is different for low WIMP mass.
- The above behavior is carried over to the total rates. For WIMP flows the maximum is in winter, but for the M-B distribution one finds the usual case (maximum in June 3rd) for low reduced mas but maximum in December for relatively large reduced mass.

Acknowledgments

JDV is indebted to the Physics Department of KAIST and IBS for their kind invitation and support and to Professor Yannis K. Semertzidis, Director of CAPP/IBS at KAIST, for useful discussions and his hospitality, while EC would like to thank Changhong Li, Jin U Kang and Konstantin Savvidy for many useful discussions. This research project has been supported in parts by the Jiangsu Ministry of Science and Technology under contract BK20131264. We also acknowledge 985 Grants from the Chinese Ministry of Education, and the Priority Academic Program Development for Jiangsu Higher Education Institutions (PAPD).

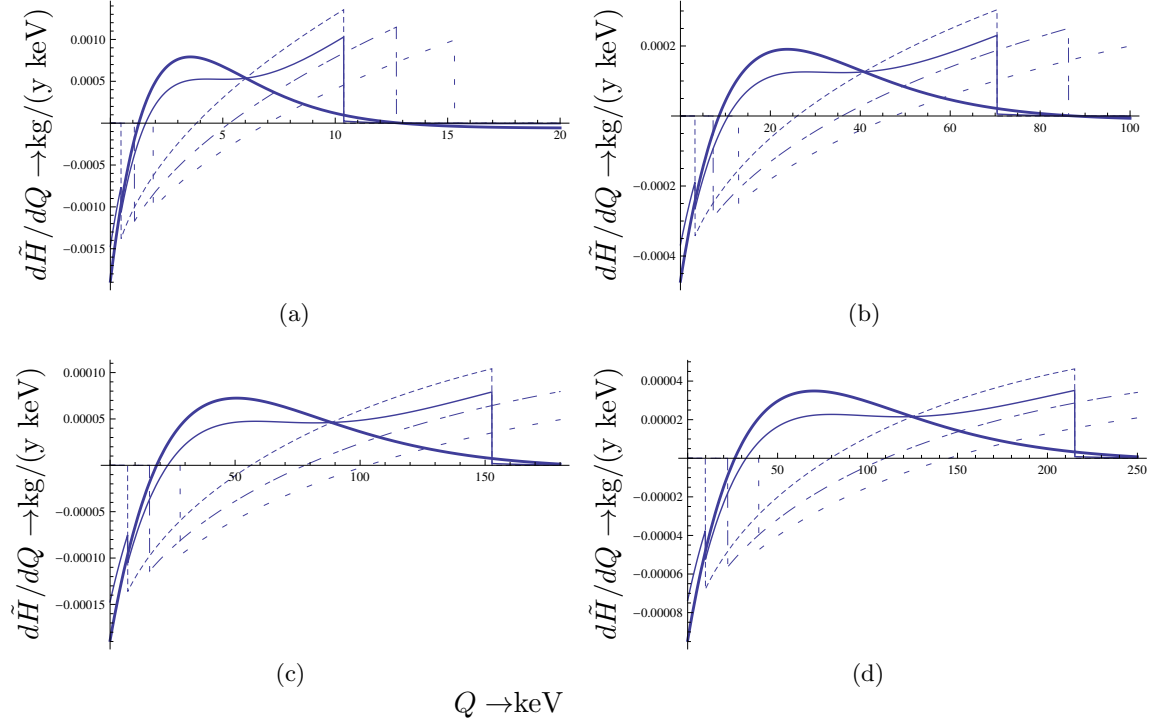


Figure 15: The differential rate $\frac{d\tilde{H}}{dQ}$, as a function of the recoil energy for a light target, e.g. ^{23}Na assuming a nucleon cross section of 10^{-8}pb . Panels (a) (b), (c) and (d) correspond to 5, 20, 50 and 100 GeV WIMP masses. Otherwise the notation is the same as that of Fig. 5.

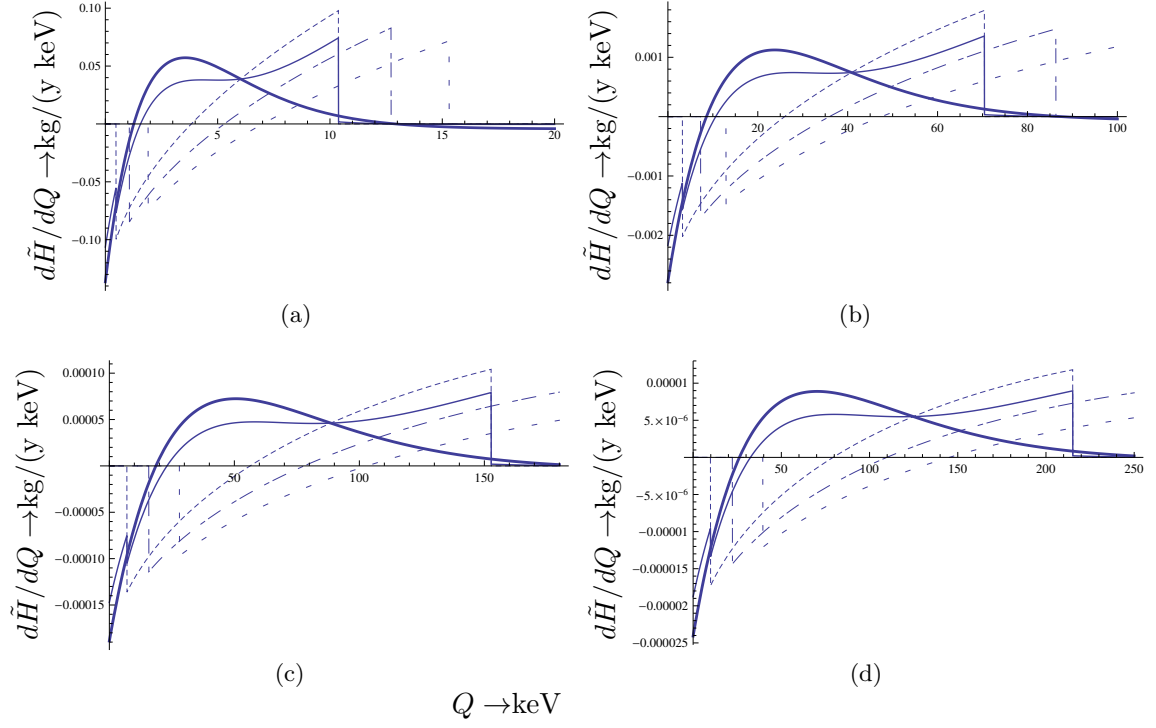


Figure 16: The same as in Fig. 12 in the case of a light target, e.g. ^{23}Na .

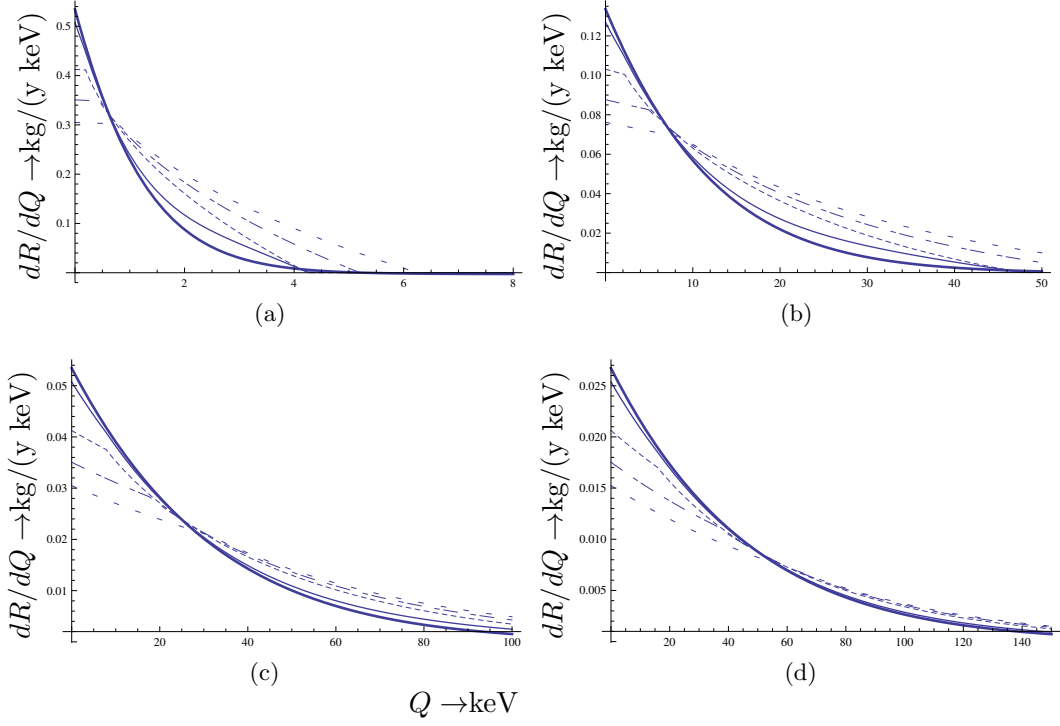


Figure 17: The differential rate $\frac{dR}{dQ}$, as a function of the recoil energy for an intermediate target, e.g. ^{73}Ge assuming a nucleon cross section of 10^{-8}pb . Panels (a) (b), (c) and (d) correspond to 5, 20, 50 and 100 GeV WIMP masses. Otherwise the notation is the same as that of Fig. 5.

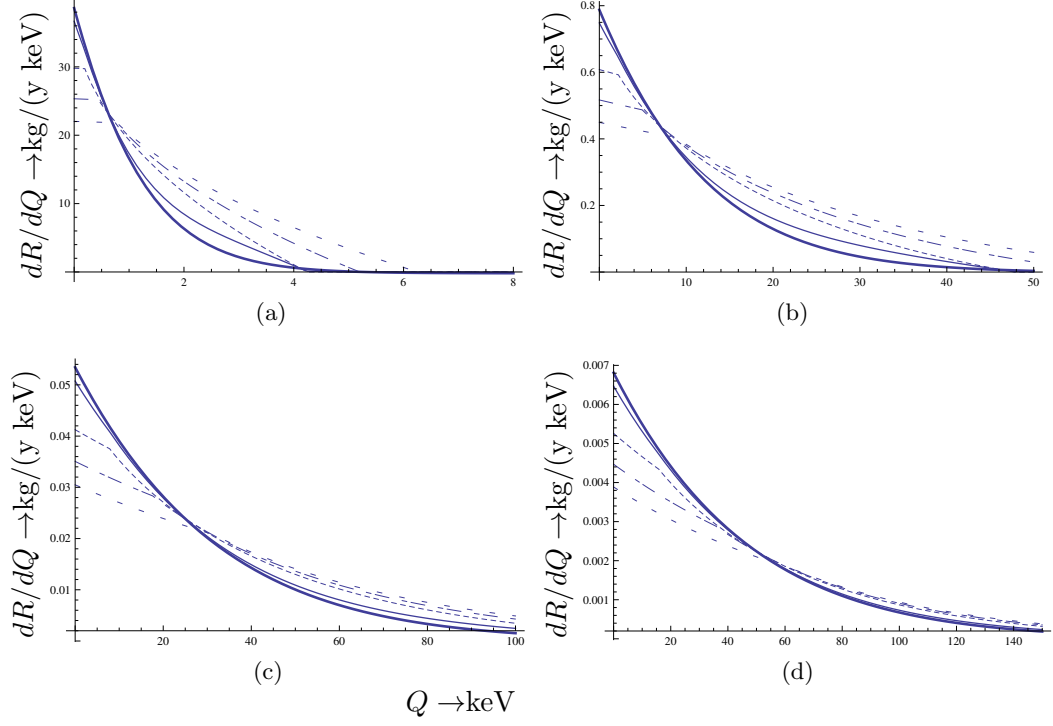


Figure 18: The same as in Fig. 10 in the case of an intermediate target, e.g. ^{73}Ge .

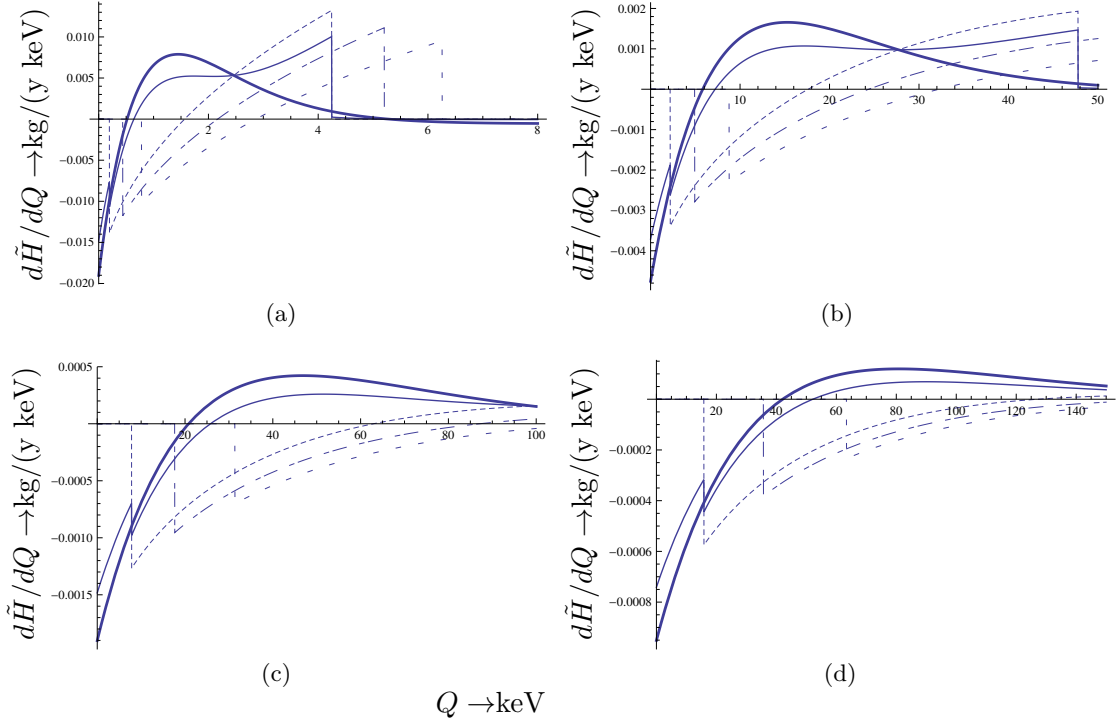


Figure 19: The differential rate $\frac{d\tilde{H}}{dQ}$, as a function of the recoil energy for an intermediate target, e.g. ^{73}Ge assuming a nucleon cross section of 10^{-8}pb . Panels (a) (b), (c) and (d) correspond to 5, 20, 50 and 100 GeV WIMP masses. Otherwise the notation is the same as that of Fig. 5.

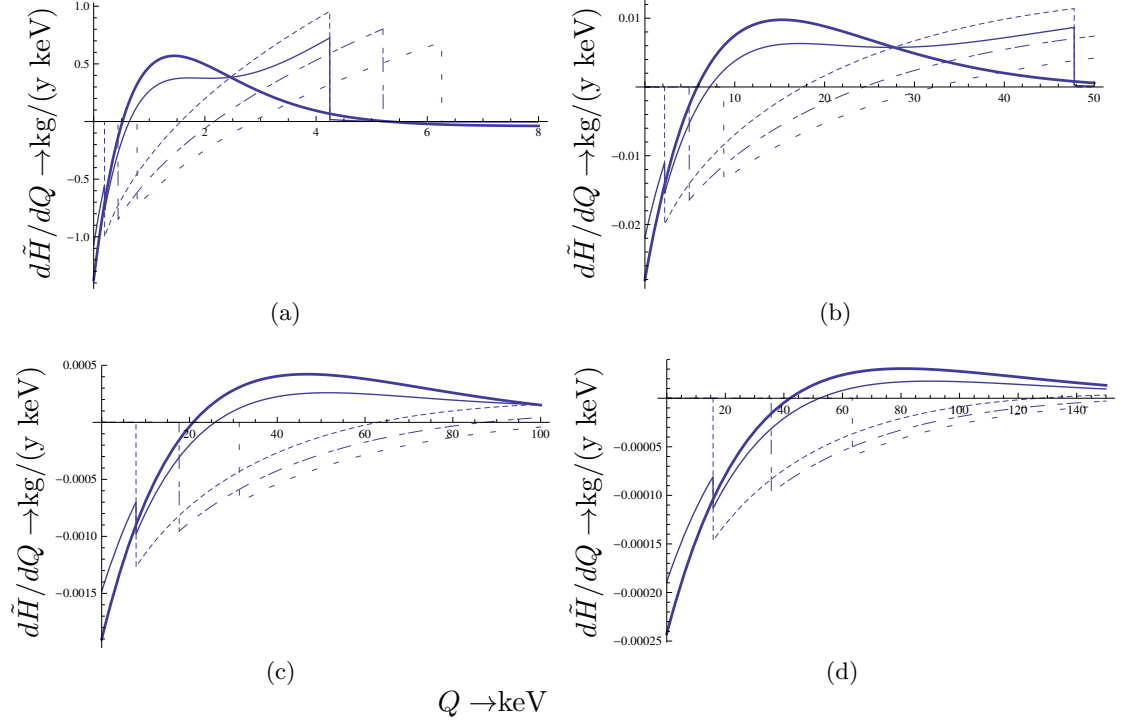


Figure 20: The same as in Fig. 12 in the case of an intermediate target, e.g. ^{73}Ge .

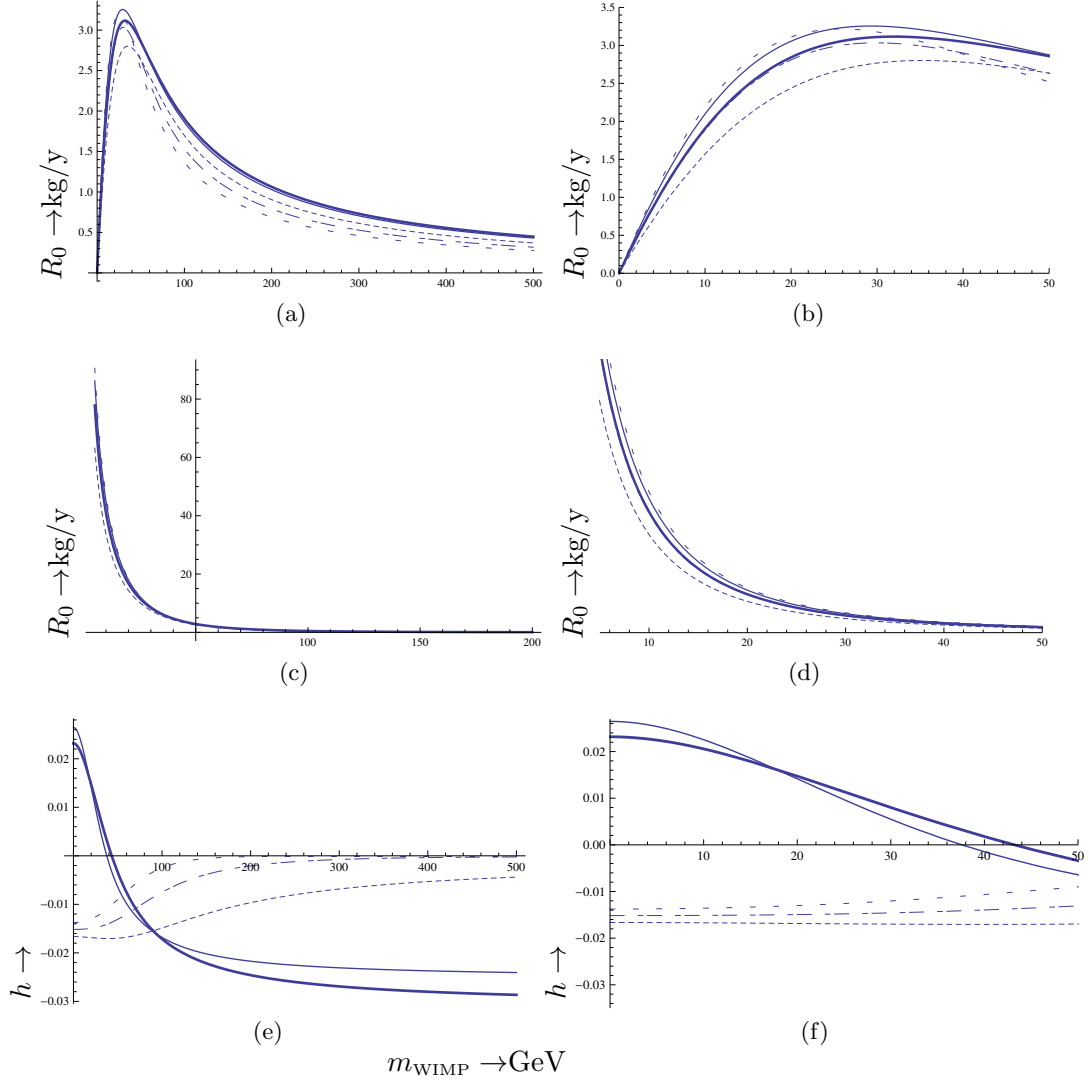


Figure 21: The total rate R_0 for usual WIMP (top panels) and and the scalar WIMP (middle panels) and the relative modulation h (bottom panels) as a function of the WIMP mass in GeV in the case of a heavy target ^{127}I at zero threshold. The panels on the right are a restriction of those on the left to smaller masses. Otherwise the notation is the same as that of Fig. 5.

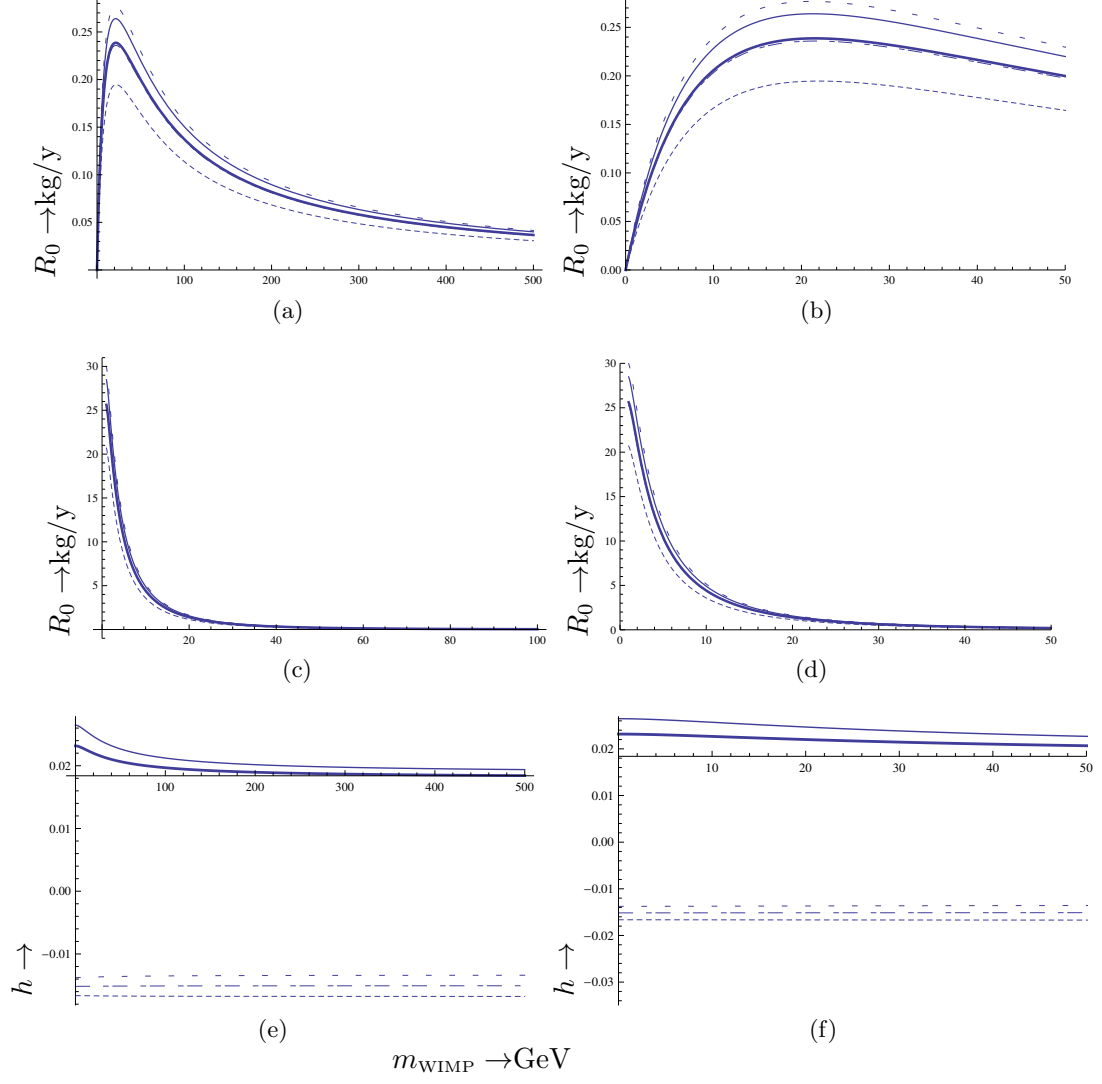


Figure 22: The same as in Fig. 21 for a light target, e.g. ^{23}Na .

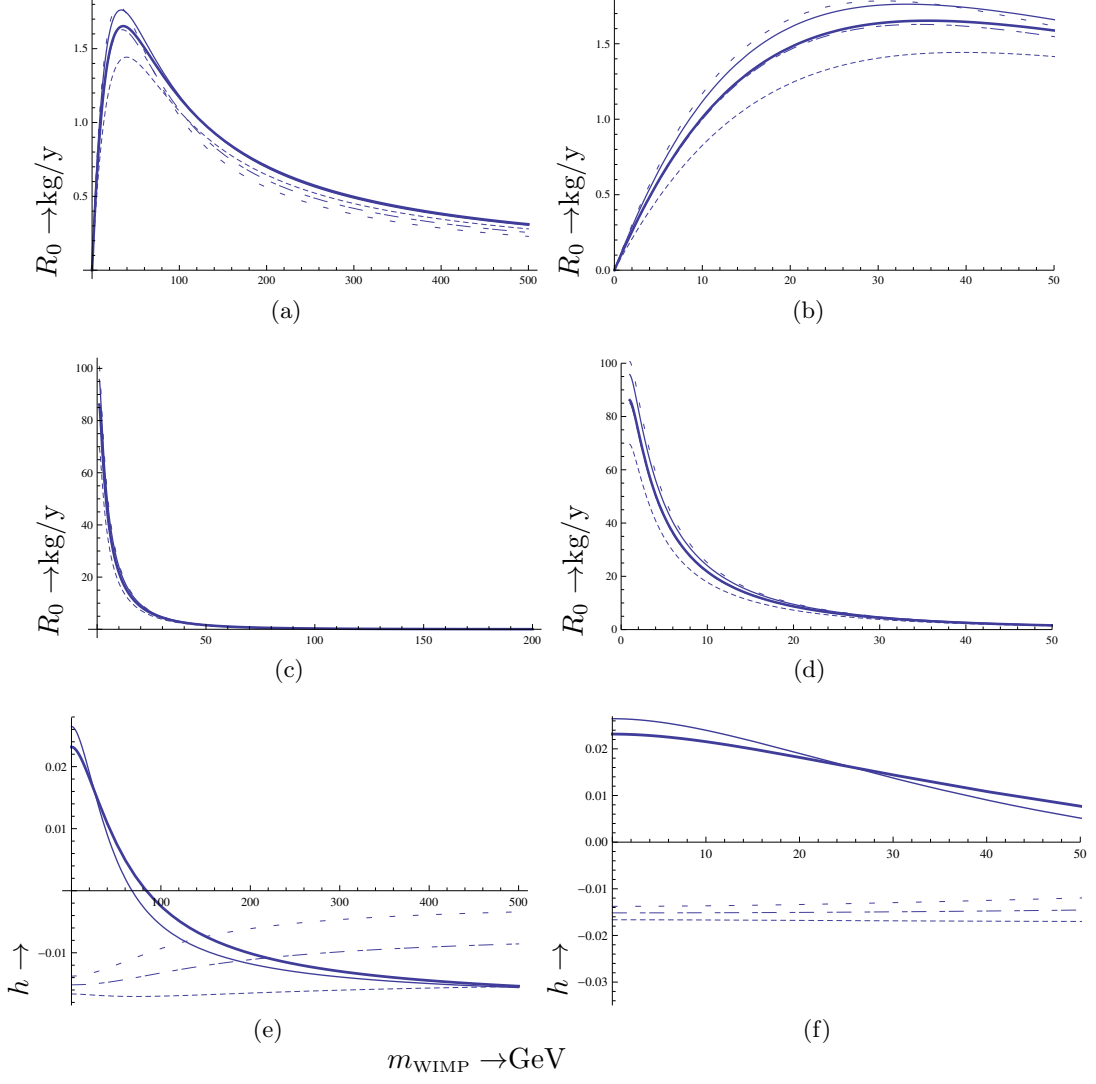


Figure 23: The same as in Fig. 21 for an intermediate target, e.g. ^{73}Ge .

References

- [1] S. Hanany and *et al* *Astrophys. J.* **545** (2000) L5.
- [2] J. Wu and *et al* *Phys. Rev. Lett.* **87** (2001) 251303.
- [3] M. Santos and *et al* *Phys. Rev. Lett.* **88** (2002) 241302.
- [4] P. D. Mauskopf and *et al* *Astrophys. J.* **536** (2002) L59.
- [5] S. Mosi and *et al* *Prog. Nuc.Part. Phys.* **48** (2002) 243.
- [6] N. W. Halverson et al. *Astrophys. J.* **568** (2002) 38.
- [7] G. F. Smoot and *et al* (COBE Collaboration) *Astrophys. J.* **396** (1992) L1.
- [8] A. H. Jaffe and *et al* *Phys. Rev. Lett.* **86** (2001) 3475.
- [9] D. N. Spergel and *et al* *Astrophys. J. Suppl.* **148** (2003) 175.
- [10] D. Spergel et al. *Astrophys. J. Suppl.* **170** (2007) 377. [arXiv:astro-ph/0603449v2].
- [11] The Planck Collaboration, A.P.R. Ade *et al*, arXiv:1303.5076 [astro-ph.CO].
- [12] D. P. Bennett and *et al* *Phys. Rev. Lett.* **74** (1995) 2867.
- [13] P. Ullio and M. Kamiokowski *JHEP* **0103** (2001) 049.
- [14] J. D. Lewin and P. F. Smith *Astropart. Phys.* **6** (1996) 87.
- [15] M. W. Goodman and E. Witten *Phys. Rev. D* **31** (1985) 3059.
- [16] A. Drukier, K. Freeze, and D. Spergel *Phys. Rev. D* **33** (1986) 3495.
- [17] J. R. Primack, D. Seckel, and B. Sadoulet *Ann. Rev. Nucl. Part. Sci.* **38** (1988) 751.
- [18] A. Gabutti and K. Schmiemann *Phys. Lett. B* **308** (1993) 411.
- [19] R. Bernabei *Riv. Nuovo Cimento* **18 (5)** (1995) 1.
- [20] D. Abriola et al. *Astropart. Phys.* **10** (1999) 133. arXiv:astro-ph/9809018.
- [21] F. Hasenbalg *Astropart. Phys.* **9** (1998) 339. arXiv:astro-ph/9806198.
- [22] J. D. Vergados *Phys. Rev. D* **67** (2003) 103003. hep-ph/0303231.
- [23] A. Green *Phys. Rev. D* **68** (2003) 023004. *ibid*: **D 69** (2004) 109902; arXiv:astro-ph/0304446.
- [24] C. Savage, K. Freese, and P. Gondolo *Phys. Rev. D* **74** (2006) 043531. arXiv:astro-ph/0607121.
- [25] P. J. Fox, J. Kopp, M. Lisanti and N. Weiner, A CoGeNT Modulation Analysis, arXiv:1107.0717 (astro-ph.CO).
- [26] D. Spergel *Phys. Rev. D* **37** (1988) 1353.
- [27] The NAIAD experiment B. Ahmed *et al*, *Astropart. Phys.* **19** (2003) 691; hep-ex/0301039
B. Morgan, A. M. Green and N. J. C. Spooner, *Phys. Rev. D* **71** (2005) 103507; astro-ph/0408047.
- [28] Y. Shimizu, M. Minoa, and Y. Inoue *Nuc. Instr. Meth. A* **496** (2003) 347.
- [29] V.A. Kudryavtsev, Dark matter experiments at Boulby mine, astro-ph/0406126.
- [30] B. Morgan, A. M. Green, and N. J. C. Spooner *Phys. Rev. D* **71** (2005) 103507. ; astro-ph/0408047.
- [31] B. Morgan and A. M. Green *Phys. Rev. D* **72** (2005) 123501.
- [32] A. M. Green and B. Morgan *Astropart. Phys.* **27** (2007) 142. [arXiv:0707.1488 (astrp-ph)].
- [33] C. Copi, J. Heo, and L. Krauss *Phys. Lett. B* **461** (1999) 43.
- [34] C. Copi and L. Krauss *Phys. Rev. D* **63** (2001) 043507.

- [35] A. Alenazi and P. Gondolo *Phys. Rev. D* **77** (2008) 043532.
- [36] R.J. Creswick and S. Nussinov and F.T. Avignone III, arXiv: 1007.0214 [astro-ph.IM].
- [37] Lisanti and J.G. Wacker, arXiv: 0911.1997 [hep-ph].
- [38] F. Mayet *et al*, Directional detection of dark matter, arXiv:1001.2983 (astro-ph.IM).
- [39] J. Vergados and D. Owen *Phys. Rev. D* **75** (2007) 043503.
- [40] J. Vergados *Astronomical Journal* **137** (2009) 10. [arXiv:0811.0382 (astro-ph)].
- [41] N. Tetradis, J. Vergados, and A. Faessler *Phys. Rev. D* **75** (2007) 023504.
- [42] J. D. Vergados, S. H. Hansen, and O. Host *Phys. Rev. D* **77** (2008) 023509.
- [43] P. Sikivie *Phys. Rev. D* **60** (1999) 063501.
- [44] P. Sikivie *Phys. Lett. B* **432** (1998) 139.
- [45] J. D. Vergados *Phys. Rev. D* **63** (2001) 06351.
- [46] A. M. Green *Phys. Rev. D* **63** (2001) 103003.
- [47] G. Gelmini and P. Gondolo *Phys. Rev. D* **64** (2001) 123504.
- [48] A. M. Green *Phys. Rev. D* **66** (2002) 083003.
- [49] M. Kuhlen et al. *JCAP* **1002** (2010) 030.
- [50] M. Lisanti, L. E. Strigari, J. G. Wacker, and R. H. Wechsler *Phys. Rev. D* **83** (2011) 023519.
- [51] K. Stewart, J. Bullock, R. Wechsler, A. Maller, and A. Zenter *Astrophys. J.* **683** (2008) 597.
- [52] C. Purcell, S. Kazantzidis, and J. Bullock *Ap. J. Lett.* **694** (2009) L98.
- [53] M. Lisanti and D.N.Spergel, Dark Matter Debris Flows in the Milky Way, arXiv:1105.4166 (astro-ph.CO).
- [54] A. Natarajan, C. Savage and Katherine Freese, arXiv:1109.0014 (astro-ph.CO) (to appear in *Phys. Rev. D*).
- [55] M. Kuhlen, M. Lisanti and D.N. Spergel, Direct Detection of Dark Matter Debris Flows, arXiv:1202.0007 (astro-ph.GA).
- [56] J. D. Vergados *Phys. Rev. D* **85** (2013) 123502. arXiv:1202.3105 [hep-ph].
- [57] C. Li, R. H. Brandenberger, and Y.-K. E. Cheung, *Big Bounce Genesis*, [arXiv:1403.5625](#).
- [58] Y.-K. E. Cheung, J. U. Kang, and C. Li, *Dark matter in a bouncing universe*, *JCAP* **1411** (2014), no. 11 001, [[arXiv:1408.4387](#)].
- [59] D. J. Chung, E. W. Kolb, and A. Riotto, *Nonthermal supermassive dark matter*, *Phys.Rev.Lett.* **81** (1998) 4048–4051, [[hep-ph/9805473](#)].
- [60] J. Angle *et al*, arXiv:1104.3088 [hep-ph].
- [61] E. Aprile et al. *Phys. Rev. Lett.* **107** (2011) 131302. arXiv:1104.2549v3 [astro-ph.CO].
- [62] C. Aalseth et al. *Phys. Rev. Lett.* **106** (2011) 131301. CoGeNT collaboration arXiv:10002.4703 [astro-ph.CO].
- [63] R. Bernabei and Others *Eur. Phys. J. C* **56** (2008) 333. [DAMA Collaboration]; [arXiv:0804.2741 [astro-ph]].
- [64] P. Belli et al. *Phys. Rev. D* **84** (2011) 05501. the DAMA collaboration, arXiv:1106.4667 [astro-ph.GA].
- [65] D.C. Malling et al, arXiv:1110.0103((astro-ph.IM)).
- [66] D. S. A. et al (CDMS Collaboration) *Phys.Rev.Lett.* **93** (2004) 211301.

- [67] The CRESST Experiment: Recent Results and Prospects, P.Di Stefano, *et al.*, arXiv:hep-ex/0011064; The CRESST Collaboration, talk presented at IBS - MultiDark Joint Focus Program, Daejeon, s. Korea, 10–21 October 2014.
- [68] S. Archambault et al. *Phys. Lett. B* **682** (2009) 185. collaboration PICASSO, arXiv:0907.0307 [astro-ex].
- [69] S. Archambault et al. *New J. Phys.* **13** (2011) 043006. arXiv:1011.4553 (physics.ins-det).
- [70] J. D. Vergados *Commun. Theor. Phys.* **57** (2012) 504. arXiv:1108.4768 (hep-ph).
- [71] V. Oikonomou, J. D. Vergados, and C. C. Moustakidis *Nuc. Phys. B* **773** (2007) 19.
- [72] C. Boehm and P. Fayet *Nucl.Phys. B* **683** (2004) 29. arXiv:hep-ph/0305261.
- [73] E. Ma *Phys. Rev. D* **73** (2006) 077301. arXiv:hep-ph/0601225.
- [74] C. Li, L. Wang, and Y.-K. E. Cheung, *Bound to bounce: A coupled scalartachyon model for a smooth bouncing/cyclic universe*, *Phys.Dark Univ.* **3** (2014) 18–33, [arXiv:1101.0202].
- [75] C. Li and Y.-K. E. Cheung, *The scale invariant power spectrum of the primordial curvature perturbations from the coupled scalar tachyon bounce cosmos*, *JCAP* **1407** (2014) 008, [arXiv:1401.0094].
- [76] D. Wands, *Duality invariance of cosmological perturbation spectra*, *Phys.Rev.* **D60** (1999) 023507, [gr-qc/9809062].
- [77] Y.-F. Cai, R. Brandenberger, and X. Zhang, *Preheating a bouncing universe*, *Phys.Lett.* **B703** (2011) 25–33, [arXiv:1105.4286].
- [78] J. Liu, Y.-F. Cai, and H. Li, *Evidences for bouncing evolution before inflation in cosmological surveys*, *J.Theor.Phys.* **1** (2012) 1–10, [arXiv:1009.3372].
- [79] Y.-F. Cai, R. Brandenberger, and X. Zhang, *The Matter Bounce Curvaton Scenario*, *JCAP* **1103** (2011) 003, [arXiv:1101.0822].
- [80] H. Li, M. Li, T. Qiu, J. Xia, Y. Piao, et al., *What can we learn from the tension between PLANCK and BICEP2 data?*, *Sci.China Phys.Mech.Astron.* **57** (2014) 1431–1441.
- [81] J. Quintin, Y.-F. Cai, and R. H. Brandenberger, *Matter Creation in a Nonsingular Bouncing Cosmology*, arXiv:1406.6049.
- [82] Y. Wan, S. Li, M. Li, T. Qiu, Y. Cai, et al., *Single field inflation with modulated potential in light of the Planck and BICEP2*, arXiv:1405.2784.
- [83] Y.-F. Cai, *Exploring Bouncing Cosmologies with Cosmological Surveys*, *Sci.China Phys.Mech.Astron.* **57** (2014) 1414–1430, [arXiv:1405.1369].
- [84] Z.-G. Liu, H. Li, and Y.-S. Piao, *Pre-inflationary genesis with CMB B-mode polarization*, arXiv:1405.1188.
- [85] M. Li, *Generating scale-invariant tensor perturbations in the non-inflationary universe*, arXiv:1405.0211.
- [86] Y.-F. Cai and Y. Wang, *Testing quantum gravity effects with latest CMB observations*, *Phys.Lett.* **B735** (2014) 108–111, [arXiv:1404.6672].
- [87] Y.-F. Cai, J. Quintin, E. N. Saridakis, and E. Wilson-Ewing, *Nonsingular bouncing cosmologies in light of BICEP2*, arXiv:1404.4364.
- [88] B. Hu, J.-W. Hu, Z.-K. Guo, and R.-G. Cai, *Reconstruction of the primordial power spectra with Planck and BICEP2*, arXiv:1404.3690.
- [89] H. Li, J.-Q. Xia, and X. Zhang, *Global fitting analysis on cosmological models after BICEP2*, arXiv:1404.0238.

- [90] J.-Q. Xia, Y.-F. Cai, H. Li, and X. Zhang, *Evidence for bouncing evolution before inflation after BICEP2*, *Phys.Rev.Lett.* **112** (2014) 251301, [[arXiv:1403.7623](#)].
- [91] Y.-F. Cai and E. Wilson-Ewing, *Non-singular bounce scenarios in loop quantum cosmology and the effective field description*, *JCAP* **1403** (2014) 026, [[arXiv:1402.3009](#)].
- [92] M. Novello and S. P. Bergliaffa *Phys. Rep.* **463** (2008) 127. [arXiv: 0802.1634](#) [astro-ph].
- [93] R. H. Brandenberger, (2012), [arXiv:1206.4196](#) [astro-ph.CO].
- [94] V. Silveira and A. Zee *Phys. Lett. B* **161** (1985) 136.
- [95] D. Holz and A. Zee *Phys. Lett. B* **517** (201) 239.
- [96] M. Bento, O. Berolami, and R. Rosefeld *Phys. Lett. B* **518** (2001) 276.
- [97] M. Bento, O. Berolami, R. Rosefeld, and L. Teodoro *Phys. Rev. D* **62** (2000) 041302.
- [98] T. P. Cheng, *Phys. Rev. D* **38**, 2869 (1988); H-Y. Cheng, *Phys. Lett. B* **219**, 347 (1989).
- [99] A. Djouadi and M. K. Drees, *Phys. Lett. B* **484**, 183 (2000); S. Dawson, *Nucl. Phys. B* **359**, 283 (1991); M. Spira et al, *Nucl. Phys.* **B453**, 17 (1995).
- [100] J. D. Vergados, On The Direct Detection of Dark Matter- Exploring all the signatures of the neutralino-nucleus interaction, [hep-ph/0601064](#).
- [101] E. Aprile et al. *Phys. Rev. Lett.* **109** (2012) 181301. [XENON100 Collaboration]; [arXiv: 1207.5988](#) (astro-ph.Co).
- [102] C. C. Moustakidis, J. D. Vergados, and H. Ejiri *Nucl. Phys. B* **727** (2005) 406. [hep-ph/0507123](#).
- [103] E. Aprile et al. *J. Phys. G: Nucl. Part. Phys.* **41** (2014) 035201. [XENON100 Collaboration]; [arXiv:1311.1088](#) (astro-ph.IM).
- [104] J. D. Vergados *Phys. Rev. D* **85** (2012) 123502. [arXiv:1202.3105](#) (hep-ph).
- [105] J. D. Vergados *Lect. Notes Phys.* **720** (2007) 69. [hep-ph/0601064](#).
- [106] J. D. Vergados and C. C. Moustakidis *Eur. J. Phys.* **9(3)** (2011) 628. [arXiv:0912.3121](#) [astro-ph.CO].
- [107] P. C. Divari, T. S. Kosmas, J. D. Vergados, and L. D. Skouras *Phys. Rev. C* **61** (2000) 054612–1.
- [108] M. T. Ressell *et al.*, *Phys. Rev. D* **48**, 5519 (1993); M.T. Ressell and D. J. Dean, *Phys. Rev. C* **56**, 535 (1997).
- [109] The PICASSO collaboration: S. Archambault *et al*, Private Communication.
- [110] R. Bernabei et al. *Eur. Phys. J. C* **73** (2013) 2648. [DAMA/LIBRA phase 1]; [arXiv:1308.5109](#) (astro-GA.).